JOURNAL OF PETROLOGY | VOLUME 47 | NUMBER 3 | PAGES 435–455 | 2006 | doi:10.1093/petrology/egi080

Evolution from Oceanic Subduction to Continental Collision: a Case Study from the Northern Tibetan Plateau Based on Geochemical and Geochronological Data

SHUGUANG SONG[1,2]*, LIFEI ZHANG[1,2], YAOLING NIU[3], LI SU[4], BIAO SONG[2] AND DUNYI LIU[2]

[1]KEY LABORATORY OF OROGENIC BELTS AND CRUSTAL EVOLUTION, SCHOOL OF EARTH AND SPACE SCIENCES, PEKING UNIVERSITY, BEIJING 100871, P.R. CHINA

[2]SHRIMP LABORATORY, INSTITUTE OF GEOLOGY, CAGS, BEIJING 100037, P.R. CHINA

[3]DEPARTMENT OF EARTH SCIENCE, DURHAM UNIVERSITY, DURHAM DH1 3LE, UK

[4]GEOLOGIC LAB CENTRE, CHINESE UNIVERSITY OF GEOSCIENCES, BEIJING 100083, P.R. CHINA

RECEIVED DECEMBER 10, 2004; ACCEPTED SEPTEMBER 30, 2005
ADVANCE ACCESS PUBLICATION OCTOBER 28, 2005

Two apparently distinct, sub-parallel, paleo-subduction zones can be recognized along the northern margin of the Tibetan Plateau: the North Qilian Suture Zone (oceanic-type) with ophiolitic mélanges and high-pressure eclogites and blueschists in the north, and the North Qaidam Belt (continental-type) in the south, an ultrahigh-pressure (UHP) metamorphic terrane comprising pelitic and granitic gneisses, eclogites and garnet peridotites. Eclogites from both belts have protoliths broadly similar to mid-ocean ridge basalts (MORB) or oceanic island basalts (OIB) in composition with overlapping metamorphic ages (480–440 Ma, with weighted mean ages of 464 ± 6 Ma for North Qilian and 457 ± 7 Ma for North Qaidam), determined by zircon U–Pb sensitive high-resolution ion microprobe dating. Coesite-bearing zircon grains in pelitic gneisses from the North Qaidam UHP Belt yield a peak metamorphic age of 423 ± 6 Ma, 40 Myr younger than the age of eclogite formation, and a retrograde age of 403 ± 9 Ma. These data, combined with regional relationships, allow us to infer that these two parallel belts may represent an evolutionary sequence from oceanic subduction to continental collision, and continental underthrusting, to final exhumation. The Qilian–Qaidam Craton was probably a fragment of the Rodinia supercontinent with a passive margin and extended oceanic lithosphere in the north, which was subducted beneath the North China Craton to depths >100 km at c. *423 Ma and exhumed at* c. *403 Ma (zircon rim ages in pelitic gneiss).*

KEY WORDS: *HP and UHP rocks; subduction belts; zircon SHRIMP ages; Northern Tibetan Plateau*

INTRODUCTION

High-pressure metamorphic rocks within orogenic belts record dynamic Earth processes of subduction and exhumation of both oceanic and continental lithospheric materials. Paleo-subduction zones identified within the continents may be divided into two types: oceanic-type and continental-type, which correspond to the Pacific-type and Alpine-type of Ernst (2001) and B-type and A-type of Maruyama *et al.* (1996), respectively. This division is convenient for distinguishing common lithological assemblages. In this study, we show that the subduction-zone complexes in the northern Tibetan plateau provide a strong case that these end-member subduction types may in fact represent an evolutionary sequence in a single subduction system from oceanic lithosphere subduction, to continental collision with underthrusting to exhumation. The tectonic sequence is consistent with the general belief that continental collision follows oceanic lithospheric subduction as exemplified by the Cenozoic Himalayan and Alpine orogenies (e.g. O'Brien, 2001).

An oceanic-type subduction zone complex, comprising fragments of oceanic lithosphere (ophiolitic mélange),

*Corresponding author. Present address: Department of Geology, Peking University, Beijing 100871, P.R. China. Telephone: +86-01-6275-1145. Fax: +86-10-6275-1159. E-mail: sgsong@pku.edu.cn

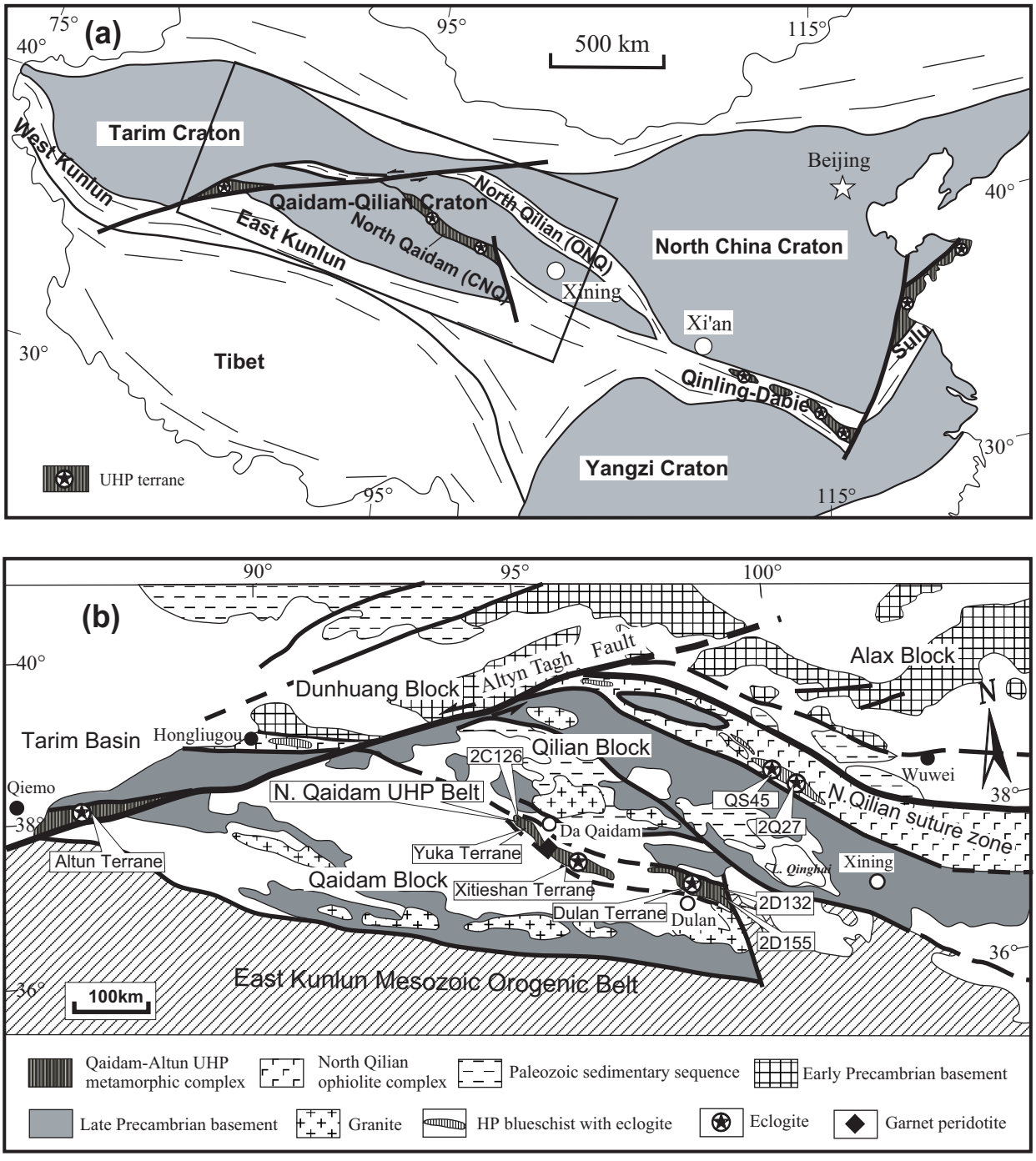

Fig. 1. Schematic maps showing major tectonic units of China (a) and subunits of the Qilian–Qaidam orogenic belts in the northern Tibetan Plateau (b). Revised after Dong *et al.* (1986).

island arc assemblages and high-pressure low-temperature blueschists and eclogites is well exposed along the North Qilian Suture Zone (Fig. 1; Wu *et al.*, 1993; Song, 1996), which is subsequently referred to as ONQ. A continental-type UHP belt, subsequently CNQ, is also identified along the North Qaidam margin (e.g. Song, 2001; Song *et al.*, 2003*a*, 2003*b*), and is characterized by ultrahigh-pressure (UHP) gneisses intercalated with minor eclogites and garnet peridotite blocks. The ONQ and CNQ trend NW–SE bounding the complex Qilian block (Fig. 1). Understanding the genetic relationship (if any) between these two belts is

not straightforward; typically they have been regarded as the products of two unrelated convergence events (e.g. Yang *et al.*, 2002*b*).

Zircon U–Pb geochronology has proved to be a powerful tool, not only in precisely dating the formation ages of HP and UHP metamorphic rocks, but also in unraveling the tectonic evolution of orogenic belts (Rubatto *et al.*, 1999; Hermann *et al.*, 2001; Katayama *et al.*, 2001). To decipher the relationship between the two belts, and to examine if there exists a progression from oceanic subduction to continental collision in the Northern Tibetan Plateau, we have selected eclogites from both belts, plus a coesite-bearing pelitic gneiss from the CNQ for zircon geochronology studies, using the combined techniques of mineral inclusion determination, cathodoluminescence (CL) image analysis and sensitive high-resolution ion microprobe (SHRIMP) dating. These age data, together with geochemical data for the eclogites from the two belts, allow us to suggest that the ONQ and the CNQ may indeed represent different evolutionary stages of a Paleozoic convergent margin between the North China Craton and the Qilian–Qaidam Craton.

TECTONIC UNITS

The Qilian–Qaidam Mountain system is located in the northern part of the Qinghai–Tibet Plateau. Tectonically, it represents a broad orogenic belt between the Alax and Qaidam blocks. To the SE is the Qinling Orogenic Belt (e.g. Ratschbacher *et al.*, 2003). The northern Tibetan Plateau can be divided into five tectonic units (Fig. 1); these are, from north to south, the Alax Block, the North Qilian oceanic-type Suture Zone or ONQ, the Qilian Block, the North Qaidam continental-type UHPM Belt or CNQ and the Qaidam Block. These units are cut by the Altyn Tagh Fault, a large NE-striking sinistral fault system in the west. Both the ONQ and CNQ belts can be traced on the west side of the fault (see Fig. 1), displaced up to 400 km to the SW (Zhang *et al.*, 2001).

Alax Block

The Alax Block in the north comprises the western part of the North China Craton, and consists predominantly of early Precambrian basement overlain by Cambrian to middle Ordovician strata typical of the North China Craton cover sequences (Bureau of Geology and Mineral Resources of Ningxia Province, 1990). To the west of the Altyn Tagh Fault is the Dunhuang Block, which is characterized by the same Archaean basement rocks found in the Alax Block (Mei *et al.*, 1998; Li *et al.*, 2001).

North Qilian Suture Zone (ONQ)

The North Qilian Suture Zone is an elongate, NW-trending belt that lies between the Alax Block (north) and the Qilian Block (south). It is made up of Early Paleozoic subduction complexes including ophiolitic mélanges, high-pressure blueschists and eclogites, island-arc volcanic rocks with granite plutons, Silurian flysch formations, Devonian molasse, and Carboniferous to Triassic sedimentary cover sequences (Feng & He, 1995; Song, 1996). The ONQ is interpreted to have formed in an 'oceanic type' subduction zone of Early Paleozoic age.

The ophiolite, which is interpreted to represent the remnants of ancient oceanic lithosphere, is well preserved in this suture zone. The basaltic rocks geochemically resemble present-day N-type and E-type mid-ocean ridge basalt (MORB) (Feng & He, 1995). Zircons from a cumulate gabbro within the ophiolite suite gave U–Pb SHRIMP magmatic ages ranging from 533 to 568 Ma (554 ± 16 Ma) (Yang *et al.*, 2002*b*). Within the suture zone are two sub-belts of high-pressure metamorphic rocks (Wu *et al.*, 1993; Song, 1996): (1) a low-grade blueschist belt with a typical assemblage of glaucophane, lawsonite, pumpellyite, aragonite, albite; (2) a high-grade blueschist belt with an assemblage of garnet, phengite, glaucophane and epidote that locally encloses massive blocks of eclogite. The protoliths of the blueschists include greywacke, marble, chert and volcanic rocks. Glaucophane and phengite Ar–Ar isotope dating has yielded ages in the range 460–440 Ma (Liou *et al.*, 1989; Wu *et al.*, 1993; Zhang *et al.*, 1997).

Qilian Block

The Qilian Block, located between the North Qilian Suture Zone (ONQ) and the North Qaidam UHP Belt (CNQ), is an imbricate thrust belt of Precambrian basement overlain by Paleozoic sedimentary sequences. The basement consists of felsic gneiss, marble, amphibolite and localized granulite. Wan *et al.* (2001) reported 910–940 Ma single-zircon ages in granitic gneisses from different regions of the north part of the Qilian Block, which were interpreted as protolith formation ages and are consistent with the ages of granitic gneisses from the North Qaidam UHP Belt (see below).

North Qaidam UHP Belt (CNQ)

The North Qaidam UHP Belt, located between the Qilian Block and Qaidam Block, consists of eclogite peridotite- and garnet peridotite-bearing terranes. From east to west, these are the Dulan terrane, Xitieshan terrane, and Yuka terrane (see Fig. 1 for localities). Magmatic zircon grains with oscillatory zoning from a granitic gneiss, the major host rock of eclogite blocks in Dulan, gave $^{206}Pb/^{238}U$ SHRIMP ages of 932–1011 Ma

Table 1: List of studied samples with mineral assemblages and localities

Sample	Rock	Mineral assemblage	Locality
ONQ			
Q35	eclogite	Grt, Omp, Phn, Gln, Ep, Rt, Qtz	N38°15′55″, E099°56′30″
QS45	eclogite	Grt, Omp, Phn, Gln, Ep, Rt	N38°16′50″, E099°55′04″
Q67	eclogite	Grt, Omp, Phn, Gln, Ep, Rt	N38°16′51″, E099°55′05″
Q70	eclogite	Grt, Omp, Phn, Gln, Ep, Rt	N38°16′50″, E099°55′04″
Q71	eclogite	Grt, Omp, Phn, Gln, Ep, Rt, Qtz	N38°16′48″, E099°55′04″
2Q27	eclogite	Grt, Omp, Phn, Gln, Ep, Rt, Qtz	N38°04′25″, E100°33′52″
Q122	eclogite	Grt, Omp, Phn, Gln, Ep, Rt, Qtz	N38°04′26″, E100°33′52″
Q125	eclogite	Grt, Omp, Phn, Gln, Ep, Rt, Qtz	N38°04′24″, E100°33′52″
Q126	eclogite	Grt, Omp, Phn, Gln, Ep, Rt, Qtz	N38°04′23″, E100°33′51″
Q127	eclogite	Grt, Omp, Phn, Gln, Ep, Rt, Qtz	N38°04′23″, E100°33′51″
Q128	eclogite	Grt, Omp, Phn, Gln, Ep, Rt, Qtz	N38°04′20″, E100°33′51″
CNQ			
2C87	eclogite	Grt, Omp, Phn, Rt, Ep	N37°55′12″, E094°56′06″
2C101	eclogite	Grt, Omp, Phn, Rt	N37°58′48″, E094°58′07″
2C102	eclogite	Grt, Omp, Phn, Rt	N37°58′49″, E094°58′03″
2C124	eclogite	Grt, Omp, Phn, Rt, Qtz	N37°59′13″, E094°53′25″
2C125	eclogite	Grt, Omp, Phn, Rt, Qtz	N37°59′13″, E094°53′25″
2C126	pelitic gneiss	Grt, Mus, Ky, Rt, Pl, Qtz	N37°59′13″, E094°53′24″
9Y117	granitic gneiss	Mus, Pl, Kfs, Qtz	N36°35′24″, E098°25′03″
2C155	eclogite	Grt, Omp, Rt, Phn,	N36°35′24″, E098°25′02″
2D132	pelitic gneiss	Grt, Mus, Ky, Rt, Aln, Pl, Qtz	N36°36′45″, E098°26′20″

Amphibole is a common retrograde phase in the CNQ eclogites. Mineral abbreviations are after Kretz (1983).

with a mean at 992 ± 40 Ma (Song, 2001), which is similar to the single-zircon ages of granitic gneisses in the Qilian Block reported by Wan *et al.* (2001). Song *et al.* (2003*a*, 2003*b*) have described the mineral assemblages, petrography, mineralogy, P–T conditions and metamorphic evolution of the Dulan UHP terrane.

Qaidam Block

The Qaidam Block to the south is a Mesozoic intracontinental basin deposited on the Precambrian crystalline basement. Zhang *et al.* (2003) reported detrital zircon SHRIMP ages mainly ranging from 1600 to 1800 Ma for a metamorphosed paragneiss from the southern part of the Qaidam Basin, and thus concluded that the Qaidam–Qilian Craton has an affinity with the Yangtze Craton.

SAMPLE DESCRIPTION

Two eclogite samples from the ONQ HP belt and one eclogite and two paragneiss samples from the North Qaidam UHP Belt were selected for zircon U–Pb dating. Eclogites from the two belts were analyzed for their bulk-rock major and trace element compositions. All studied samples with mineral assemblages and localities are listed in Table 1.

Eclogites from the North Qilian Suture Zone (ONQ) occur as lenses within intensely foliated blueschists. The eclogite samples have a coarse-grained granular texture with a mineral assemblage involving garnet, omphacite, phengite and rutile with or without clinozoisite and quartz. Garnet is characterized by high almandine (Alm 61·5–65·8 mol %) and low pyrope (Pyr 7·3–16·0 mol %) contents. Omphacite has a high jadeite component (35·8–41·4 mol %) and phengite has high silica characteristics (Si = 3·42–3·48 p.f.u.). All the samples studied have been recrystallized to various extents by blueschist-facies retrograde metamorphism. Using the compositions of coexisting omphacite, phengite and the garnet rims in which the omphacite inclusions occur, we obtained peak eclogite-facies conditions of P = 1·8–2·5 GPa and T = 460–550°C by garnet–omphacite–phengite geothermobarometry (Ravna & Terry, 2004).

Eclogites from the North Qaidam UHP Belt (CNQ), on the other hand, occur as lenses of various sizes within granitic and pelitic gneisses in all three eclogite-bearing terranes of Dulan, Xitieshan and Yuka–Luliangshan. In the North Dulan Belt (NBD), Yuka–Luliangshan terrane

and Xitieshan terrane, they show a medium- to coarse-grained, granular, texture and have mineral assemblages involving garnet, omphacite, rutile and phengite with or without zoisite, whereas in the South Dulan Belt (SDB) they have assemblages involving garnet, omphacite, kyanite, rutile and phengite. Evidence for UHP metamorphism in the eclogites from the Dulan terrane was described by Song *et al.* (2003*a*); this includes (1) inclusions of quartz pseudomorphs after coesite and polycrystalline K-feldspar + quartz in garnet and omphacite, and (2) P–T conditions of $P = 2{\cdot}9$–$3{\cdot}3$ GPa and $T = 630$–750°C estimated by garnet–omphacite–phengite–kyanite thermobarometry (Ravna & Terry, 2004). Peak conditions of the Yuka eclogite are also within the stability field of coesite.

The paragneiss from the CNQ is usually intercalated with eclogite blocks. Sample 2D132 contains a mineral assemblage of garnet (~15–20%), muscovite (~40%), kyanite (5–10%), zoisite/allanite (<5%), quartz (~30%) and feldspar (5%), suggesting a pelitic protolith. Sample 2C126 consists of garnet (~10%), muscovite (10–15%), feldspar (5–10%) and quartz (60–70%), and is most likely to be a metamorphosed greywacke. Coesite inclusions in zircon grains from the pelitic gneiss (Song, 2001; Yang *et al.*, 2002*a*; Song *et al.*, 2003*a*, 2003*b*) demonstrate that zircon growth occurred during ultrahigh-pressure metamorphism. The comparatively low-pressure matrix mineral assemblage, on the other hand, suggests that the pelitic gneiss experienced amphibolite-facies retrogression.

ANALYTICAL METHODS

All samples were crushed and sieved to <300 μm. Zircon grains were separated magnetically, using heavy liquids, and finally hand-picked under a binocular microscope. They were then embedded in 25 mm epoxy discs and polished down to half-sections. Mineral inclusions were identified by laser Raman microspectroscopy. The internal structure of zircon grains was examined using CL and back-scattered electron (BSE) images at Peking University. The CL images were obtained by scanning electron microscopy (SEM) using a FEI PHILIPS XL30 SFEG instrument with 2 min scanning time at conditions of 15 kV and 120 nA. The zircon grains were analysed for U, Th and Pb using SHRIMP II at the SHRIMP Laboratory in the Chinese Academy of Geological Sciences, Beijing. Instrumental conditions, data acquisition and reduction were the same as those described by Compston *et al.* (1992). The data were collected in sets of five scans through the masses with 2 nA primary O_2^- beams. A reference zircon was analyzed first and then after every three analyses of unknowns. The measured $^{206}Pb/^{238}U$ ratio in the samples was corrected using reference zircon standard SL13 from a pegmatite from Sri Lanka ($^{206}Pb/^{238}U = 0{\cdot}0928$; 572 Ma) and zircon standard TEMORA (417 Ma) from Australia (Black *et al.*, 2003). The common-Pb correction used the $^{206}Pb/^{204}Pb$ ratio and assumed a two-stage evolution model (Stacey & Kramers, 1975). The measured ^{204}Pb values in the unknowns were similar to those recorded for the standard zircon and so common-Pb corrections were made assuming an isotopic composition of Broken Hill lead. The analytical data were treated following Compston *et al.* (1992) and are graphically presented on Tera–Wasserburg (TW) diagrams (Tera & Wasserburg, 1972) with 1σ errors. The mean ages are weighted means calculated using Isoplot (Ludwig, 1991) at the 95% confidence level.

Whole-rock major element analyses for eclogites were performed on a Perkin Elmer Optima 3300 DV inductively coupled plasma optical emission spectrometry (ICP-OES) system at The University of Queensland (Niu, 2004) and by X-ray fluorescence (XRF) at Northwest University, Xi'an, China (Rudnick *et al.*, 2004). Trace element analyses were carried out by inductively coupled plasma mass spectrometry (ICP-MS) using a Fisons PQ2 system at The University of Queensland, Australia (e.g. Niu & Batiza, 1997) and an Elan 6100-DRC system at Northwest University, Xi'an, China (e.g. Rudnick *et al.*, 2004). Representative data are given in Table 2. For the major elements, precision (RSD) is better than 6% and accuracy is better than 4%, and for trace elements, precision is generally better than 5% for most elements and accuracy is better than 10%, with many elements agreeing to within 2% of the reference values.

The $^{40}Ar/^{39}Ar$ analyses were performed at the Institute of Geology of the Chinese Academy of Geological Sciences, using the same analytical procedure as described by Gao & Klemd (2003). The data are presented in Table 5 (below). The errors are given as 2σ. Mineral inclusions in zircon crystals were detected using laser Raman microspectroscopy (Ranisow RM-1000) with the 514·5 nm line of an Ar-ion laser at Peking University.

GEOCHEMISTRY OF ECLOGITES FROM THE TWO BELTS

The major and trace element compositions of the eclogites from the ONQ HP and the CNQ UHP belts are broadly similar (Table 2), with the exception that the CNQ eclogite has a higher CaO content than the ONQ eclogite. In FeO_t/MgO vs TiO_2 and V vs Ti discrimination diagrams, most samples with relatively low Ti (TiO_2 <2·0 wt %) from both belts fall in the field of MORB, whereas those with high Ti (TiO_2 >2·0 wt %) plot in the field of within-plate basalts (WPB) (Fig. 2). Eclogites from both belts show similar ranges of variation in light rare earth elements (LREE) (Fig. 3a and c),

Table 2: Representative major and trace element analyses of eclogites from the ONQ HP and CNQ UHP belts

	Eclogites from the ONQ HP belt									Eclogites from the CNQ UHP belt				
Sample:	Q35*	Q67*	Q70*	Q71*	Q122†	Q125†	Q126†	Q127†	Q128†	2C87*	2C101*	2C102*	2C124*	2C125*†
Major elements (wt %)														
SiO_2	46·83	45·43	49·5	52·47	49·83	49·22	47·99	48·16	45·78	45·52	46·19	45·99	49·37	48·45
TiO_2	2·05	2·98	1·31	1·31	1·33	1·59	1·64	1·73	1·56	3·38	2·60	2·52	1·38	1·38
Al_2O_3	14·62	16·15	13·12	13·48	19·28	18·61	15·87	16·81	16·14	15·51	15·07	15·26	14·83	15·18
FeO_t	15·59	11·75	12·38	10·72	10·44	11·35	10·91	14·82	12·19	14·62	14·60	13·87	13·07	12·95
MnO	0·26	0·15	0·2	0·14	0·16	0·18	0·21	0·37	0·20	0·20	0·21	0·19	0·22	0·20
MgO	5·13	4·71	6·5	6·98	4·60	5·57	6·63	7·27	7·15	6·10	6·70	6·38	7·07	7·31
CaO	6·74	7·52	7·84	4·32	7·52	7·74	8·61	6·75	7·95	10·04	10·88	10·63	11·38	11·40
Na_2O	0·24	2·47	3·92	4·48	1·10	2·87	2·80	2·45	1·80	3·34	2·32	2·44	2·85	3·20
K_2O	2·18	3·4	1·66	2·93	2·61	1·11	1·15	1·35	1·00	0·76	0·55	0·93	0·04	0·02
P_2O_5	0·3	0·68	0·14	0·11	0·39	0·20	0·25	0·43	0·25	0·37	0·31	0·31	0·12	0·13
LOI	4·31	3·44	2·15	2·17						0·18	0·46	1·00	0·20	0·26
Total	98·25	98·68	98·72	99·11	97·26	98·45	96·06	100·15	94·00	100·02	99·89	99·52	100·13	100·48
ppm														
La	21·27	34·90	13·71	8·19	5·26	4·60	4·90	7·61	7·12	20·2	15·80	15·82	6·78	6·35
Ce	46·29	73·34	28·78	17·65	13·71	14·15	15·18	18·39	18·24	45·3	35·4	35·4	14·9	13·2
Pr	4·35	6·50	2·67	1·78	2·12	2·28	2·49	2·64	2·68	6·36	4·94	4·92	2·23	1·96
Nd	21·34	29·63	13·45	10·19	10·16	11·23	11·99	11·87	12·39	27·7	21·7	21·6	10·18	8·33
Sm	5·11	6·24	3·64	2·85	3·21	3·51	3·69	3·43	3·66	6·12	5·10	5·09	2·95	2·22
Eu	1·71	2·21	1·30	1·10	1·19	1·34	1·32	1·23	1·29	2·17	1·75	1·74	0·97	0·73
Gd	7·15	6·72	5·53	3·81	0·76	0·79	0·82	0·87	0·84	5·82	5·18	5·09	3·63	3·17
Tb	1·09	0·85	0·94	0·71	4·22	4·47	4·67	4·60	4·80	0·86	0·83	0·78	0·73	0·68
Dy	6·88	4·27	5·02	4·17	5·13	5·21	5·31	6·06	5·62	4·72	4·70	4·62	4·71	4·64
Ho	1·45	0·90	1·07	0·87	1·09	1·13	1·18	1·44	1·25	0·94	0·93	0·91	1·05	1·03
Er	3·77	2·18	3·07	2·35	3·00	3·24	3·43	4·41	3·70	2·31	2·34	2·33	2·75	2·77
Tm	0·54	0·28	0·46	0·35	0·42	0·47	0·50	0·68	0·58	0·32	0·33	0·34	0·43	0·43
Yb	3·69	1·89	3·23	2·33	2·62	2·99	3·14	4·40	3·79	2·16	2·17	2·19	2·84	2·93
Lu	0·61	0·31	0·54	0·38	0·39	0·45	0·46	0·68	0·57	0·33	0·33	0·33	0·45	0·45
Ba	672·4	1238	247·2	953	259·25	89·38	87·80	152·37	261·90	255·26	118·43	160·67	22·03	16·46
Co	41·85	42·84	40·39	34·7	55·77	40·92	43·89	40·95	41·21	85·72	143·74	86·09	140·02	106·32
Cr	208	68	102	64	329·50	315·50	277·61	284·50	162·38	77·93	90·62	86·85	171·09	177·37
Ni	142	69	61	35	111·90	97·73	115·69	114·78	56·26	72·78	60·45	54·38	50·46	45·12
Sr	56·86	140·1	51·4	184·9	436·95	205·70	124·15	176·43	301·09	347·13	255·24	274·22	57·93	77·25
V	248·7	258	357	325·2	143·40	213·48	218·75	228·97	247·94	332·30	338·73	327·69	320·86	352·38
Sc	45·33	25·67	47·65	37·66	37·52	36·64	33·95	40·37	38·20	27·05	36·01	33·99	48·65	47·75
Zr	163	117	115	72	78·22	105·26	116·02	114·69	102·63	167·70	137·51	143·79	95·55	96·15
Hf	4·7	3·3	3·5	2·2	2·16	2·63	2·91	3·08	2·73	4·35	3·61	3·76	2·70	2·75
Nb	26	10	6·5	3·2	2·73	3·40	4·15	4·60	3·95	24·56	21·79	21·75	8·16	10·13
Rb	52	92	41	107	65·24	15·14	17·32	19·38	22·18	16·35	23·61	68·86	1·55	0·86
Ta	3·5	1·1	1·7	0·3	0·17	0·22	0·27	0·27	0·23	1·68	1·58	1·53	0·69	0·73
Th	3·7	9·6	5·9	1·2	0·80	0·27	0·34	1·18	1·02	1·84	1·45	1·48	1·35	1·87
U	0·7	2·9	1·4	0·6	0·31	0·10	0·11	0·50	0·31	0·76	0·52	0·56	1·81	0·95
Y	35·35	20·15	26·85	21·20	27·33	28·18	29·32	35·99	30·97	25·21	26·10	25·14	29·60	29·82
ΣREE	125·25	170·22	83·41	56·73	53·29	55·87	59·07	68·30	66·52	125·36	101·49	101·18	54·56	48·87

*Samples were analysed by XRF for major elements and ICP-MS for trace elements at Northwest University, China.
†Samples were analysed by ICP-OES for major elements and ICP-MS for trace elements at The University of Queensland, Australia.

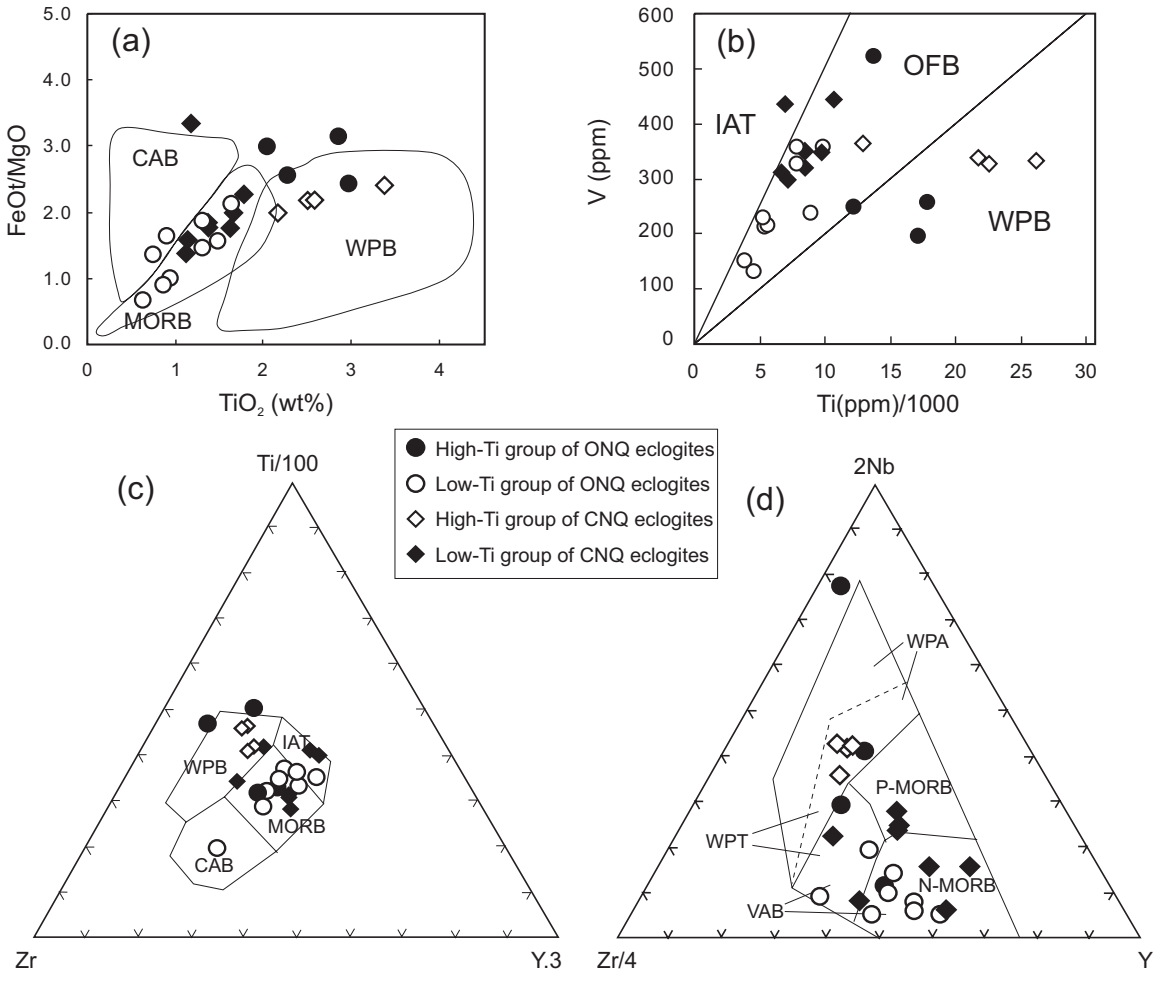

Fig. 2. Discrimination diagrams for eclogites from the North Qilian oceanic-type belt (ONQ) and the North Qaidam continental-type UHP belt (CNQ). (a) TiO_2 vs FeO_t/MgO diagram after Glassiey (1974) (FeO_t as total Fe); (b) Ti vs V diagram after Shervais (1982); (c) Ti–Zr–Y diagram after Pearce & Cann (1973); (d) Nb–Zr–Y diagram after Meschede (1986). CAB, calc-alkaline basalt; MORB, mid-ocean ridge basalt; IAT, island-arc tholeiite; OFB, ocean-floor basalt; WPA, within-plate alkalic basalt; WPB, within-plate basalt; WPT, within-plate tholeiite; VAB, volcanic arc basalt; P-MORB, plume MORB; N-MORB, normal MORB.

resembling the patterns for depleted N-type to enriched basalts of near-ridge seamounts or ocean island basalt (OIB) (Niu & Batiza, 1997). The samples with TiO_2 >2·0 wt % (e.g. Q35 and Q67 from the North Qilian HP belt and 2C87, 2C101 and 2C102 from the North Qaidam UHP Belt) have high overall REE abundances (ΣREE) and show strong LREE enrichment in chondrite-normalized REE diagrams (Fig. 3a and c). In primitive mantle normalized trace element variation diagrams (Fig. 3b and d), these rocks show geochemical characteristics similar to OIB or E-type MORB (Bernard-Griffiths & Cornichet, 1985; Sun & McDonough, 1989; Niu & Batiza, 1997). The samples with comparatively lower contents of TiO_2 have low overall REE abundance, consistent with N-type MORB compositions in primitive mantle normalized trace element diagrams and in trace element discrimination diagrams [e.g. Ti vs V, Shervais (1982) (Fig. 2b), Ti–Zr–Y, Pearce & Cann (1973) and Nb–Zr–Y, Meschede (1986) (Fig. 2c and d)].

ZIRCON U–Pb GEOCHRONOLOGY

Eclogites from the North Qilian oceanic-type belt (ONQ)

Two eclogite samples QS45 (from the same location as Q67 and Q68) and 2Q27 (from the same location as Q98–126) from the North Qilian HP belt were studied for zircon U–Th–Pb SHRIMP geochronology. Zircon grains recovered from these two samples are colorless, round to ovoid crystals and have a diameter of ~100 μm. Rare garnet and omphacite inclusions were identified by Raman microspectroscopy (Fig. 4a and b). The CL images show that some zircon grains contain a small (10–20 μm

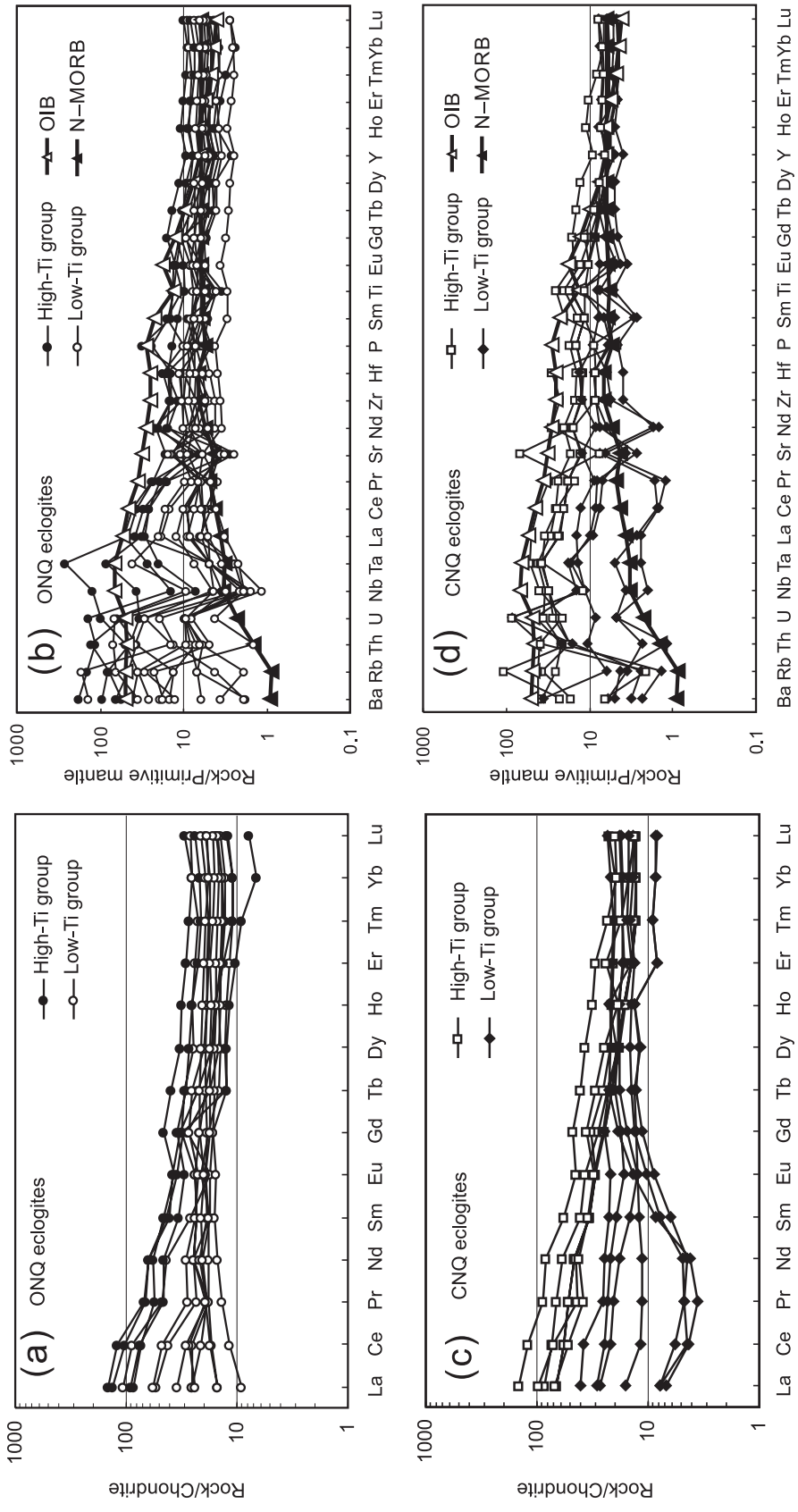

Fig. 3. Chondrite-normalized REE patterns and primitive mantle-normalized trace element diagrams for eclogites from the North Qilian (a, b) and the North Qaidam belts (c, d). Data for Dulan eclogites are from Song *et al.* (2003*b*). Chondrite and primitive mantle abundances are from Sun & McDonough (1989).

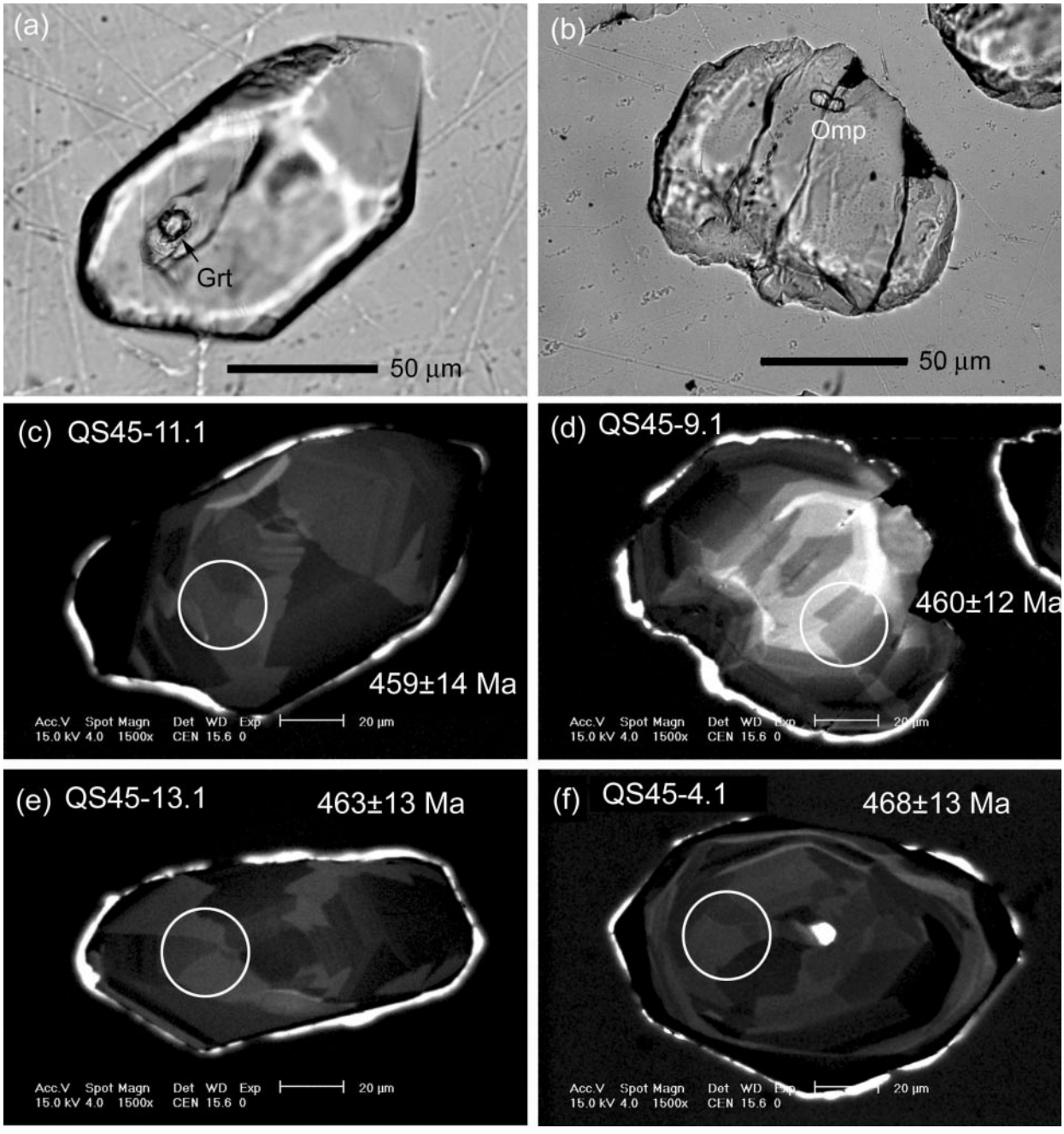

Fig. 4. Photomicrographs of zircon from the ONQ eclogites showing mineral inclusions, cathodoluminescence (CL) images, and SHRIMP ages: (a) garnet (Grt) inclusion in zircon (QS45) (plane-polarized light); (b) omphacite inclusion in zircon (QS45) (plane-polarized light); (c) CL image of (a); (d) CL image of (b); (e, f) CL images. It should be noted that CL images from (c) to (f) show fir-tree and radial sector zoning.

in diameter) relict core with bright luminescence. As shown in Fig. 4c–f, the major domains of all zircon grains show rather heterogeneous growth textures including fir-tree sector zoning, planar growth banding and radial sector zoning, which are interpreted as reflecting a fluctuating growth rate in a strongly changing or changed environment (Vavra *et al.*, 1996) or having formed in the presence of a fluid phase (Rubatto *et al.*, 1999; Rubatto & Gebauer, 2000). The uranium content in zircon varies significantly from 341 to 1328 ppm with Th/U ratios of 0·24–0·56. Analyses of 18 zircon grains in the two samples gave $^{206}Pb/^{238}U$ ages ranging from 449 to 476 Ma, with a mean at 464 ± 5·5 Ma (MSWD = 0·36) (Table 3; Fig. 5a). One small zircon (<50 μm) gave an age of

Table 3: U–Th–Pb SHRIMP data for zircon in eclogites from the ONQ HP and the CNQ UHP belts

Spot	U (ppm)	Th (ppm)	Th/U	$^{206}Pb^*$ (ppm)	Common Pb (%)	$^{206}Pb^*/^{238}U$	$^{207}Pb^*/^{206}Pb^*$	$^{206}Pb^*/^{238}U$ age (Ma)
Eclogites from the ONQ HP belt								
QS45-1.1	343	126	0·37	21·8	0·32	0·0736 ± 0·0021	0·0583 ± 0·0020	458 ± 12
QS45-2.1	515	168	0·33	33·0	0·15	0·0745 ± 0·0020	0·0594 ± 0·0009	463 ± 12
QS45-3.1	474	150	0·32	31·4	0·09	0·0770 ± 0·0021	0·0598 ± 0·0010	478 ± 13
QS45-4.1	350	113	0·32	22·7	0·18	0·0753 ± 0·0021	0·0563 ± 0·0013	468 ± 13
QS45-5.1	341	142	0·42	22·5	0·27	0·0766 ± 0·0022	0·0593 ± 0·0014	476 ± 13
QS45-6.1	982	427	0·43	62·5	0·16	0·0739 ± 0·0020	0·0579 ± 0·0007	460 ± 12
QS45-7.1	341	138	0·40	21·9	0·09	0·0746 ± 0·0021	0·0636 ± 0·0012	464 ± 13
QS45-8.1	1328	478	0·36	82·4	0·04	0·0721 ± 0·0023	0·0580 ± 0·0006	449 ± 14
QS45-9.1	474	114	0·24	30·2	0·19	0·0740 ± 0·0020	0·0566 ± 0·0013	460 ± 12
QS45-10.1	229	90	0·39	15·1	0·59	0·0760 ± 0·0022	0·0576 ± 0·0021	472 ± 13
QS45-11.1	381	142	0·37	24·2	0·28	0·0737 ± 0·0023	0·0577 ± 0·0013	459 ± 14
QS45-12.1	398	178	0·45	25·3	0·35	0·0738 ± 0·0021	0·0571 ± 0·0016	459 ± 12
QS45-13.1	367	155	0·42	23·6	0·46	0·0745 ± 0·0021	0·0576 ± 0·0012	463 ± 13
QS45-14.1	704	220	0·31	44·6	0·13	0·0736 ± 0·0023	0·0577 ± 0·0010	458 ± 14
QS45-15.1	403	159	0·39	25·6	0·16	0·0737 ± 0·0021	0·0571 ± 0·0010	459 ± 12
2Q27-2.1	621	335	0·56	36·1	0·11	0·0679 ± 0·0019	0·0572 ± 0·0009	423 ± 12
2Q27-3.1	510	133	0·26	33·1	0·00	0·0753 ± 0·0021	0·0588 ± 0·0009	468 ± 12
2Q27-4.1	372	146	0·39	24·2	0·11	0·0754 ± 0·0021	0·0587 ± 0·0011	469 ± 13
2Q27-6.1	644	182	0·28	41·3	0·14	0·0745 ± 0·0020	0·0584 ± 0·0009	463 ± 12
Eclogite from the CNQ UHP belt								
2D155-1.1	140	19	0·14	8·6	0·40	0·0709 ± 0·0020	0·0563 ± 0·0018	442 ± 12
2D155-2.1	132	82	0·64	8·3	1·10	0·0723 ± 0·0021	0·0483 ± 0·0037	450 ± 13
2D155-2.2	156	43	0·29	9·2	0·89	0·0683 ± 0·0020	0·0549 ± 0·0031	426 ± 12
2D155-3.1	109	11	0·10	6·8	0·59	0·0723 ± 0·0023	0·0544 ± 0·0030	450 ± 14
2D155-4.1	138	4	0·03	8·8	1·98	0·0727 ± 0·0022	0·0543 ± 0·0032	452 ± 13
2D155-5.1	140	77	0·57	9·1	1·44	0·0750 ± 0·0022	0·0501 ± 0·0023	466 ± 13
2D155-6.1	75	10	0·14	4·8	2·25	0·0730 ± 0·0023	0·0535 ± 0·0068	454 ± 14
2D155-7.1	131	92	0·72	8·6	0·00	0·0766 ± 0·0023	0·0617 ± 0·0018	476 ± 14
2D155-8.1	188	115	0·63	11·6	1·02	0·0712 ± 0·0021	0·0514 ± 0·0041	444 ± 12
2D155-9.1	124	74	0·62	8·4	0·53	0·0777 ± 0·0023	0·0548 ± 0·0024	482 ± 14
2D155-10.1	82	57	0·71	5·2	0·77	0·0730 ± 0·0024	0·0574 ± 0·0044	454 ± 14
2D155-11.1	164	4	0·03	10·6	0·31	0·0750 ± 0·0022	0·0560 ± 0·0020	466 ± 13
2D155-12.1	59	1	0·01	4·0	11·71	0·0706 ± 0·0029	0·0532 ± 0·0026	440 ± 18
2D155-13.1	102	27	0·27	6·6	1·26	0·0748 ± 0·0022	0·0539 ± 0·0034	465 ± 13
2D155-14.1	101	41	0·42	6·1	0·38	0·0708 ± 0·0022	0·0566 ± 0·0023	441 ± 13
2D155-15.1	156	96	0·63	9·8	0·81	0·0756 ± 0·0051	0·0532 ± 0·0043	470 ± 31

Radiogenic lead Pb* corrected for common Pb using ^{204}Pb. All errors are 1σ of standard deviation.

422 ± 11 Ma, which may either represent a period of zircon growth subsequent to the HP zircon generation or be caused by subsequent Pb loss.

Eclogites from the North Qaidam continental-type UHP belt (CNQ)

Eclogite sample 2D155 is from the Dulan UHP terrane of the CNQ UHP belt. Zircon grains in this sample are colorless and ovoid in shape with a diameter of ~100 μm, and morphologically resemble eclogitic zircon grains from the ONQ samples QS45 and 2Q27. CL images show stubby textures of fir-tree and radial sector zoning in most zircon grains, similar to zircon from granulite-facies rocks (Vavra *et al.*, 1996) and eclogites or gabbros (Rubatto *et al.*, 1999; Rubatto & Gebauer, 2000). Eclogite-facies mineral inclusions, such as garnet, omphacite and rutile, and rarely phengitic mica, were identified in the major domains of some zircon grains by Raman spectroscopy and electron microprobe (Fig. 6a–d and Fig. 7a and b). SHRIMP analyses of 15 zircon grains yield $^{206}Pb/^{238}U$ ages ranging from 440 to 482 Ma with a mean at 457 ± 7 Ma (MSWD = 0·91, Fig. 5b), essentially the same as the zircon SHRIMP ages of the ONQ HP eclogite samples. This age is also consistent with the whole-rock–garnet–omphacite Sm–Nd isochron ages (458 ± 10 Ma and 459 ± 3 Ma)

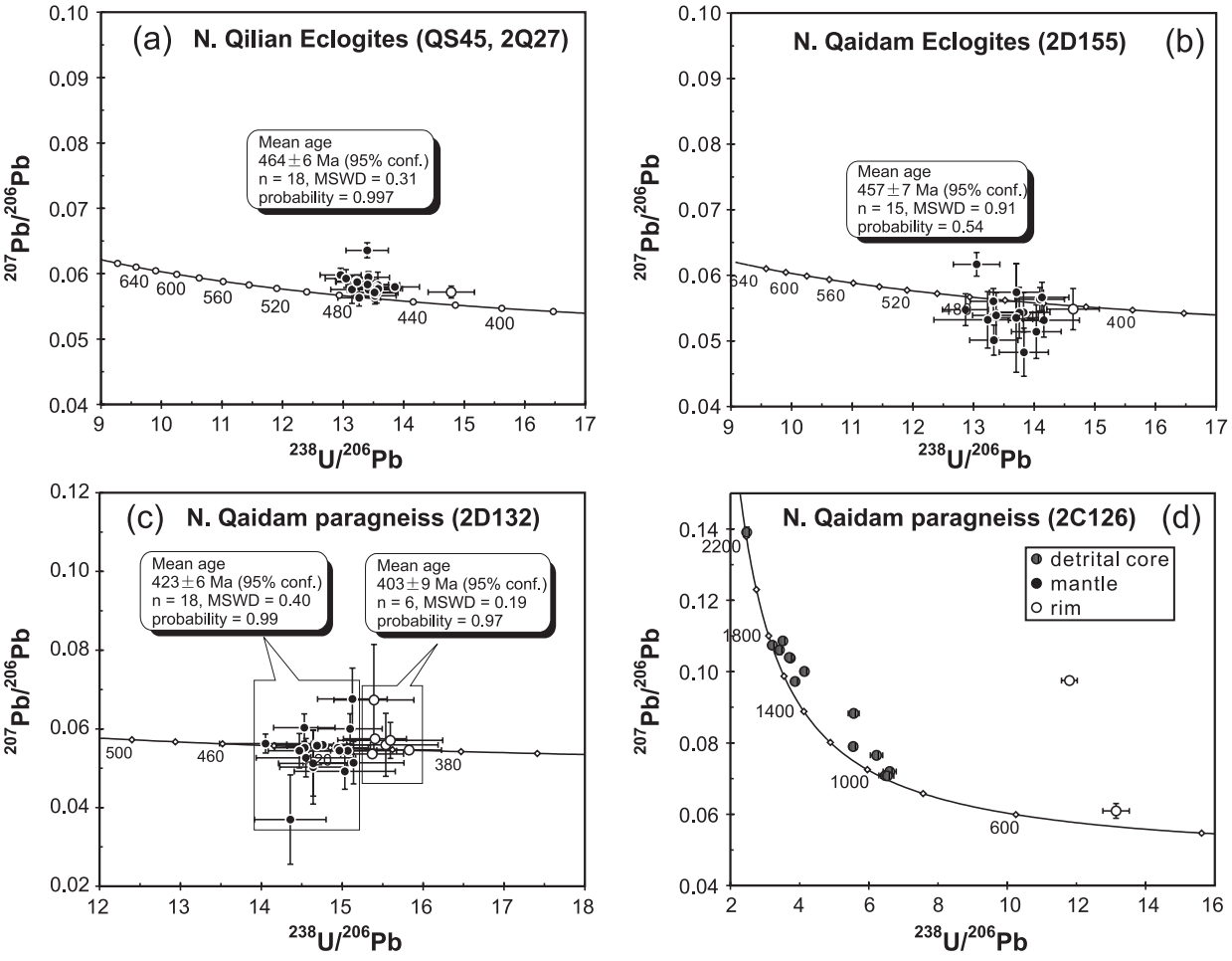

Fig. 5. Tera–Wasserburg (TW) diagrams for zircons from: (a) eclogites (QS45 and 2Q27) from the North Qilian Suture Zone (ONQ); (b) eclogite 2D155 from the North Qaidam UHP Belt (CNQ); (c) coesite-bearing pelitic gneiss from the Dulan terrane, the North Qaidam UHP Belt; (d) pelitic gneiss from the Yuka terrane, the North Qaidam UHP Belt. All plotted data are corrected using ^{204}Pb and mean ages are $^{206}Pb/^{238}U$ at the 95% confidence level. ○, rims; ●, mantles.

of the same eclogite bodies in the Dulan terrane (Song *et al.*, 2003*b*). All zircon grains from the North Qaidam UHP eclogite possess a thin bright luminescence rim (Fig. 6c–f), suggesting an overgrowth or Pb loss during a late-stage metamorphic event, but only one rim was wide enough for a SHRIMP analysis; this yielded a $^{206}Pb/^{238}U$ age of 426 ± 12 Ma (Table 3; Fig. 6f).

Paragneisses from the North Qaidam continental-type belt (CNQ)

Samples 2D132 (from the Dulan terrane) and 2C126 (from the Yuka terrane) are paragneisses that host eclogite blocks within the CNQ UHP belt. Zircon grains from these two paragneiss samples are oval and 80–150 μm in size. In sample 2D132, garnet, rutile, kyanite, phengitic mica and coesite inclusions have been reported, using Raman spectroscopy, in the mantle domains of the zircon separates (Song, 2001; Yang *et al.*, 2002*a*; Song *et al.*, 2003*a*), and were also observed as part of this study (Fig. 8, and their Raman spectra in Fig. 7c and d). As shown in Fig. 8a, b and d, the zircon grains usually contain a small detrital core with low-pressure phase inclusions (e.g. quartz or feldspar). CL images of sample 2D132 show that most zircon grains possess a relatively bright rim (Fig. 9a, c and e). In sample 2C126, most of the zircon crystals have relict cores that may reflect multiple sources for the original sedimentary protoliths. The metamorphic rims, which contain garnet, rutile and phengitic mica inclusions (Fig. 8f), are too thin (<20 μm) to be properly analyzed using the SHRIMP technique. The detrital cores, some of which show oscillatory banding in both optical microscopy and CL images (Figs 8f and 9f) and contain low-pressure inclusions of quartz and feldspar, yield a range of $^{206}Pb/^{238}U$ ages between

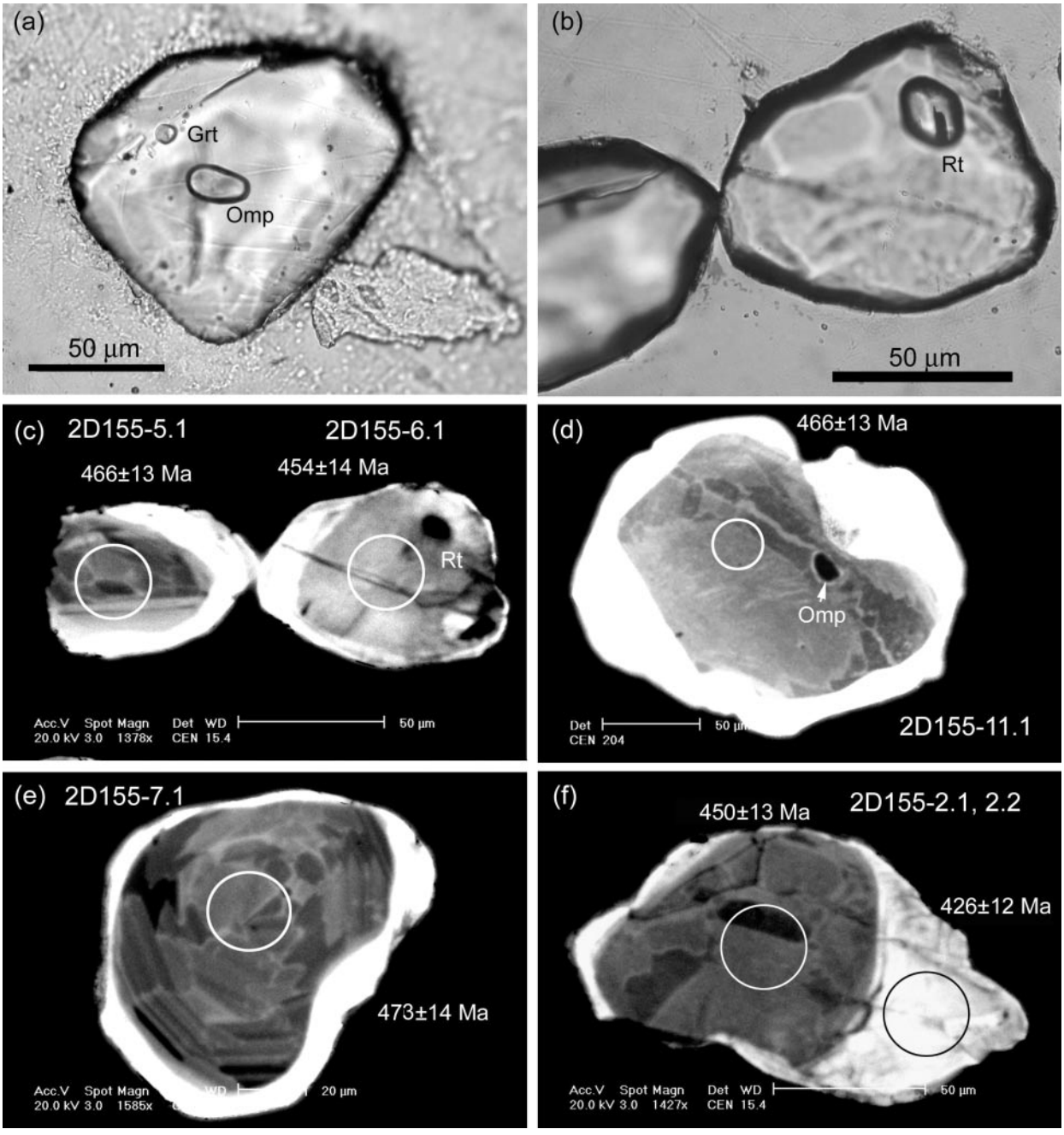

Fig. 6. Photomicrographs of zircons from the CNQ eclogites showing mineral inclusions, cathodoluminescence (CL) images, and SHRIMP ages: (a) garnet (Grt) and omphacite (Omp) inclusions in zircon (plane-polarized light); (b) rutile (Rt) inclusion in zircon (plane-polarized light); (c)–(f) CL images showing fir-tree and radial sector zones and bright luminescent rims. Zircons in (c) are the same crystals as in (b).

2192 and 909 Ma (Table 4), suggesting that they must have been sourced from Proterozoic basement. The coesite-bearing mantle domains in 2D132 show relatively weak luminescence with planar growth banding, and give a mean age of 423 ± 6 Ma ($n = 18$, MSWD = 0·32) with Th/U <0·01 (Table 4; Fig. 5c). This age is much younger than that of the eclogites from both belts. However, the presence of coesite inclusions in zircon mantle domains (Fig. 8a–e) suggests that the ~423 Ma age represents the UHP metamorphic event. The rim zircon domains from sample 2D132 yield ages of 403 ± 9 Ma (MSWD = 0·2), which reflect subsequent zircon growth because of the presence of quartz inclusions possibly during exhumation to crustal levels.

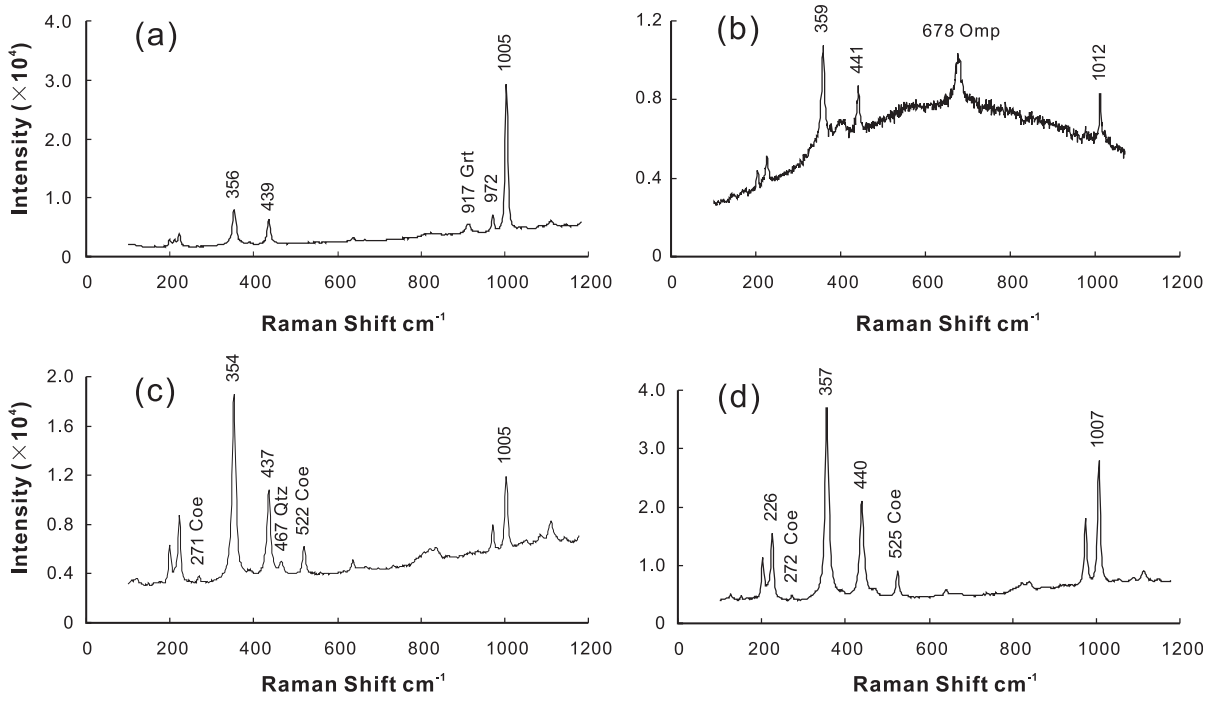

Fig. 7. Laser Raman spectroscopic analysis of inclusions in zircon from eclogite and pelitic gneiss in the North Qaidam UHP Belt (CNQ). (a) Garnet (Grt) inclusion in zircon from eclogite sample 2D155; (b) omphacite inclusion in zircon from 2D155; (c) and (d) coesite (Coe) inclusions in zircon from pelitic gneiss 2D132.

DISCUSSION

Oceanic lithosphere subduction at ~460 Ma

The protoliths of the eclogites from both the ONQ HP belt and the CNQ UHP belt are broadly similar geochemically, resembling depleted N-type to enriched E-type MORB, near-ridge seamount basalts or OIB. In two eclogite samples QS45 and 2Q27 from the North Qilian Suture Zone (ONQ), the oval morphology, internal structures shown by CL images, and mineral inclusions suggest that the zircon grains are of metamorphic origin and crystallized at eclogite-facies conditions. Eighteen analyses yield ages ranging from 476 to 449 Ma with a mean of 464 ± 5·5 Ma, corresponding to the middle Ordovician. Eclogite (2D155) from the North Qaidam UHP Belt (CNQ) also gives zircon SHRIMP $^{206}Pb/^{238}U$ ages ranging from 440 to 482 Ma, with a mean of 457 ± 7 Ma, believed to be that of the eclogite-facies metamorphic event, based on CL imaging and mineral inclusions of garnet, omphacite and rutile, with or without phengite. The strongly luminescent rims around all the zircon grains from 2D155 suggest that they were strongly influenced by a late event (probably Pb loss) during continental subduction, as discussed below. The similarity in protoliths and overlapping metamorphic ages of the ONQ and the CNQ constrain the time of the ancient oceanic lithospheric subduction to have been at ~460 Ma.

UHP metamorphism of continental material at ~423 Ma

Zircon grains from the two paragneiss samples 2D132 and 2C126 from the CNQ are distinct: zircon grains from 2D132 (pelite) are mostly newly grown with small detrital cores and wide metamorphic rims, whereas zircon grains from 2C126 (greywacke) possess very thin metamorphic rims <20 μm. As indicated by Rubatto & Gebauer (2000), the formation of a metamorphic zircon domain can occur either by new growth from a metamorphic fluid or recrystallization of a primary magmatic or detrital crystal. The fluid content and composition of the protoliths can largely constrain the growth rate and size of zircon during solid-state metamorphism.

Coesite, garnet and kyanite inclusions in the mantles of zircon grains in 2D132 suggest that they formed at UHP metamorphic conditions within the coesite stability field. CL images show metamorphic features of irregular, cloudy-zoned or fir-tree zoning patterns with Th/U <0·01. Eighteen concordant analyses for the coesite-bearing domains yielded an age of 423 ± 6 Ma. This age records a geologically significant event of UHP metamorphism in the CNQ and is consistent with the peak metamorphic ages of garnet lherzolite (423 ± 5 Ma) and garnet-bearing dunite (420 ± 5 Ma) in the same belt (Song *et al.*, 2005*b*).

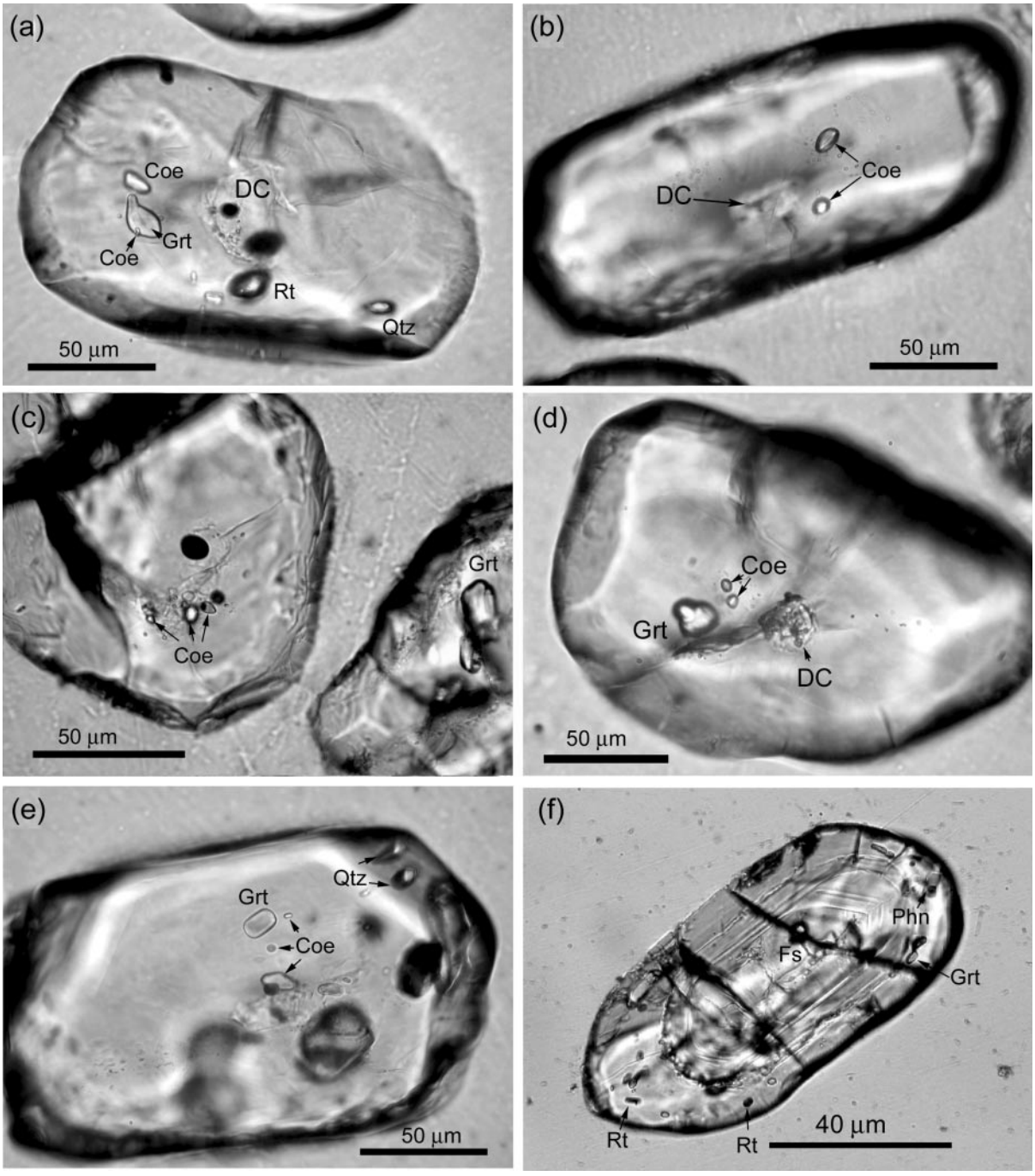

Fig. 8. Photomicrographs of zircon grains from the CNQ paragneisses. (a) Coesite (Coe) + garnet (Grt) + rutile (Rt) inclusions in the mantle domain and a quartz (Qtz) inclusion at the rim (2D132); (b) coesite inclusions and a small relict detrital core (DC) (2D132); (c) coesite inclusions in one grain and garnet inclusion in another (2D132); (d) coesite + garnet inclusions and a small relict detrital core (2D132); (e) zircon with coesite + garnet inclusions in the mantle domain and quartz inclusions at the rim (2D132); (f) a detrital magmatic core containing feldspar (Fs) and a thin metamorphic rim containing garnet, rutile and phengite (Phn) inclusions (2C126). All are plane-polarized light.

Retrogression at ~400 Ma

The rims of six zircon grains yield an age of 403 ± 9 Ma (Early–Middle Devonian), which apparently reflects a retrograde metamorphic event as shown by the growth textures of quartz and white mica (Raman spectra cannot resolve phengite or muscovite). This age is also consistent with the retrograde ages defined by the garnet peridotites (397 ± 6 Ma; Song *et al.*, 2005*b*).

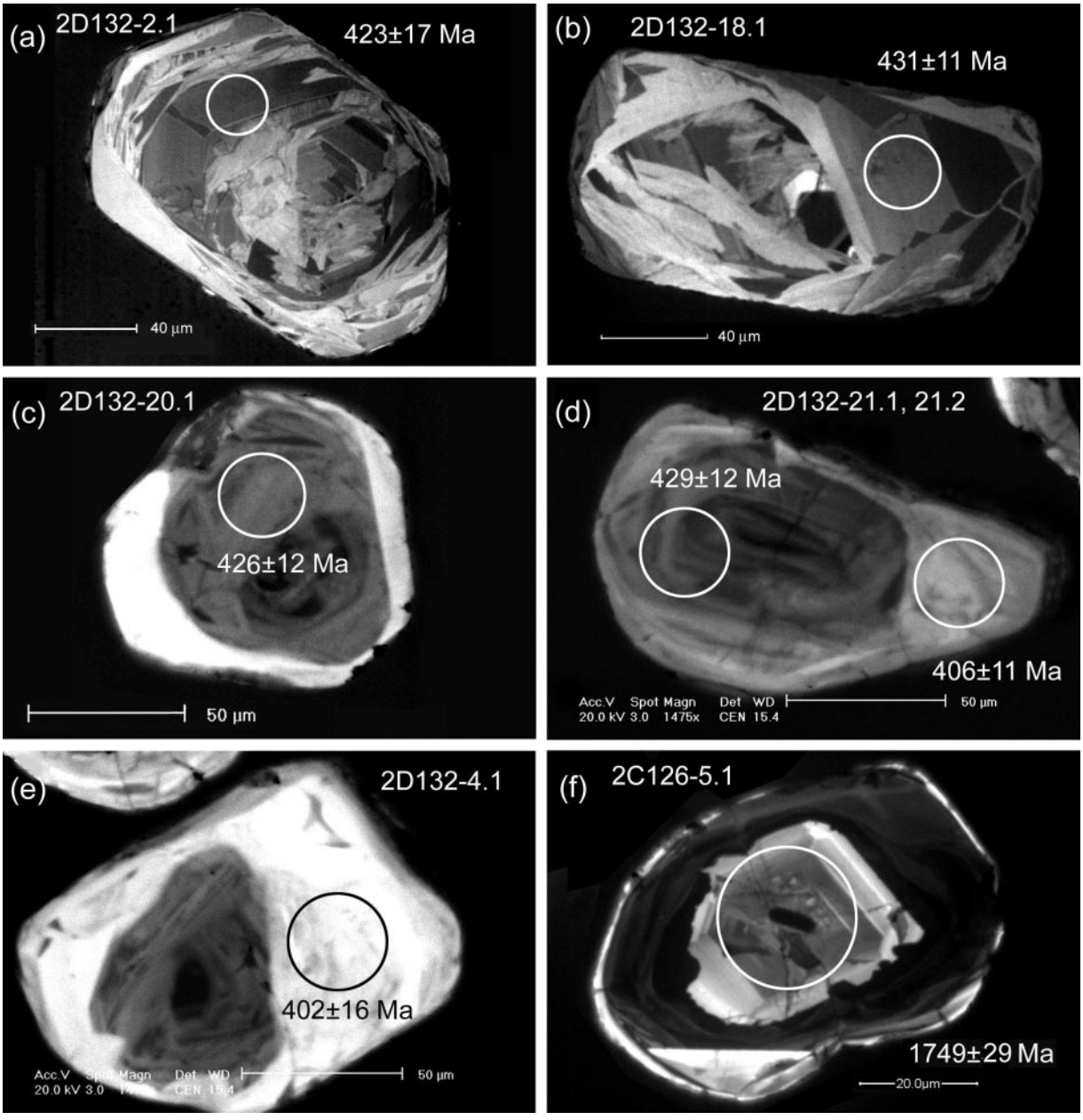

Fig. 9. Cathodoluminescence (CL) images of zircon grains, with SHRIMP age, for paragneisses from the CNQ UHP belt. (a) CL image of zircon in Fig. 8a; (b) CL image of zircon in Fig. 8b; (c) CL image of zircon in Fig. 8c; (d) CL image of zircon in Fig. 8d; (e) CL image of zircon with a wide rim (2D132); (f) CL image of zircon with a magmatic core (2C126).

White micas were recovered from a granitic gneiss (Sample 9Y117), the host rock of eclogites in the Dulan terrane of the CNQ, for $^{40}Ar/^{39}Ar$ age dating in the Isotope Laboratory, Institute of Geology, Chinese Academy of Geosciences. The $^{40}Ar/^{39}Ar$ data are given in Table 5. A well-defined plateau age of 401·5 ± 1·6 Ma was obtained from seven out of a total of 11 steps with 84·1% ^{39}Ar release (Fig. 10). Based on these concordant ~400 Ma ages, we conclude that retrogression or cooling followed the UHP event in the Early Devonian.

Tectonic evolution of the North Qilian oceanic-type suture zone (ONQ)

The North Qilian Mountains consist mostly of a number of ophiolite suites, island arc volcanic rocks and

Table 4: U–Th–Pb SHRIMP data for zircon in paragneisses from the CNQ UHP belt

Spot	U (ppm)	Th (ppm)	Th/U	$^{206}Pb^*$ (ppm)	Common Pb (%)	$^{206}Pb^*/^{238}U$	$^{207}Pb^*/^{206}Pb^*$	$^{206}Pb^*/^{238}U$ age (Ma)	$^{207}Pb^*/^{206}Pb^*$ age (Ma)
Paragneiss from greywacke									
2C126-2.1	249	127	0·53	51·9	0·15	0·2418 ± 0·0047	0·1000 ± 0·0009	1396 ± 24	1625 ± 18
2C126-3.1	859	84	0·10	198·0	0·06	0·2681 ± 0·0051	0·1038 ± 0·0004	1531 ± 26	1693 ± 8
2C126-4.1	153	82	0·56	53·4	0·09	0·4050 ± 0·0079	0·1391 ± 0·0014	2192 ± 36	2216 ± 18
2C126-5.1	506	457	0·93	135·6	0·07	0·3118 ± 0·0060	0·1074 ± 0·0005	1749 ± 29	1756 ± 8
2C126-6.1	931	132	0·15	144·4	0·15	0·1802 ± 0·0034	0·0790 ± 0·0007	1068 ± 19	1172 ± 17
2C126-7.1	193	121	0·65	48·8	0·27	0·2929 ± 0·0057	0·1061 ± 0·0013	1656 ± 28	1733 ± 22
2C126-8.1	710	1430	2·08	52·0	0·52	0·0848 ± 0·0016	0·0975 ± 0·0010	525 ± 10	1577 ± 18
2C126-9.1	651	102	0·16	159·3	0·10	0·2846 ± 0·0054	0·1086 ± 0·0005	1615 ± 27	1776 ± 8
2C126-10.1	444	342	0·79	98·7	0·07	0·2585 ± 0·0050	0·0972 ± 0·0007	1482 ± 25	1572 ± 13
2C126-11.1	816	32	0·04	108·4	0·11	0·1544 ± 0·0044	0·0709 ± 0·0005	925 ± 25	954 ± 16
2C126-12.1	487	115	0·24	63·5	0·23	0·1515 ± 0·0043	0·0720 ± 0·0008	909 ± 24	986 ± 22
2C126-13.1	840	224	0·28	129·8	0·08	0·1797 ± 0·0051	0·0883 ± 0·0005	1066 ± 28	1389 ± 11
2C126-14.1	342	51	0·15	22·5	0·78	0·0761 ± 0·0022	0·0609 ± 0·0021	473 ± 13	637 ± 73
2C126-15.1	898	136	0·16	208·8	0·15	0·2703 ± 0·0077	0·1040 ± 0·0006	1542 ± 39	1696 ± 10
2C126-16.1	677	36	0·06	93·5	0·05	0·1607 ± 0·0046	0·0765 ± 0·0005	960 ± 25	1109 ± 14
2C126-17.1	649	19	0·03	85·4	0·15	0·1530 ± 0·0044	0·0708 ± 0·0007	918 ± 25	950 ± 21
Paragneiss from pelite									
2D132-1.1	634	0·7	0·001	36·3	0·44	0·0664 ± 0·0027	0·0544 ± 0·0011	414 ± 16	
2D132-2.1	819	1·6	0·002	47·8	0·25	0·0678 ± 0·0027	0·0559 ± 0·0008	423 ± 17	
2D132-3.1	117	0·6	0·005	6·7	1·49	0·0665 ± 0·0028	0·0492 ± 0·0045	415 ± 17	
2D132-4.1	191	0·9	0·005	11·1	4·88	0·0644 ± 0·0027	0·0559 ± 0·0080	402 ± 16	
2D132-5.1	171	0·8	0·005	9·9	1·80	0·0661 ± 0·0027	0·0514 ± 0·0054	412 ± 17	
2D132-6.1	229	1·5	0·007	14·1	0·53	0·0712 ± 0·0029	0·0563 ± 0·0024	443 ± 18	
2D132-7.1	76	0·5	0·006	4·5	1·29	0·0687 ± 0·0029	0·0527 ± 0·0049	428 ± 18	
2D132-8.1	112	0·5	0·005	6·3	1·53	0·0641 ± 0·0027	0·0571 ± 0·0046	401 ± 16	
2D132-9.1	1055	0·9	0·001	59·0	0·13	0·0651 ± 0·0016	0·0536 ± 0·0007	406 ± 10	
2D132-10.1	917	1·2	0·001	51·5	0·63	0·0649 ± 0·0016	0·0575 ± 0·0008	405 ± 10	
2D132-11.1	815	0·6	0·001	47·1	0·49	0·0669 ± 0·0017	0·0552 ± 0·0009	418 ± 10	
2D132-12.1	977	1·2	0·001	57·9	0·28	0·0688 ± 0·0018	0·0552 ± 0·0007	429 ± 11	
2D132-13.1	1346	4·4	0·003	73·7	0·76	0·0632 ± 0·0016	0·0546 ± 0·0009	395 ± 10	
2D132-14.1	1082	8·2	0·008	62·4	0·37	0·0668 ± 0·0017	0·0545 ± 0·0008	417 ± 10	
2D132-15.1	1012	3·2	0·003	59·5	0·49	0·0681 ± 0·0017	0·0561 ± 0·0008	425 ± 11	
2D132-16.1	1267	1·9	0·002	74·4	0·36	0·0681 ± 0·0017	0·0557 ± 0·0007	425 ± 10	
2D132-17.1	89	0·6	0·007	5·5	3·79	0·0696 ± 0·0021	0·0370 ± 0·0114	434 ± 12	
2D132-18.1	237	0·9	0·004	14·3	1·62	0·0691 ± 0·0018	0·0544 ± 0·0044	431 ± 11	
2D132-19.1	345	1·1	0·003	20·1	1·99	0·0662 ± 0·0017	0·0600 ± 0·0038	413 ± 11	
2D132-20.1	180	0·6	0·004	11·2	5·60	0·0683 ± 0·0019	0·0503 ± 0·0094	426 ± 12	
2D132-21.1	363	0·9	0·003	21·9	2·03	0·0688 ± 0·0018	0·0603 ± 0·0035	429 ± 11	
2D132-21.2	116	0·8	0·007	6·9	5·45	0·0650 ± 0·0021	0·0673 ± 0·0141	406 ± 11	
2D132-22.1	102	0·6	0·006	6·2	3·71	0·0683 ± 0·0020	0·0512 ± 0·0083	426 ± 12	
2D132-23.1	127	0·7	0·006	7·6	5·09	0·0661 ± 0·0019	0·0676 ± 0·0079	413 ± 11	

Radiogenic lead Pb* corrected for common Pb using ^{204}Pb. All errors are 1σ of standard deviation.

Table 5: Analytical data of ^{39}Ar–^{40}Ar incremental heating experiment for the muscovite in granitic gneiss 9Y117 from the CNQ UHP belt

Release T (°C)	$^{40}Ar/^{39}Ar$	$^{36}Ar/^{39}Ar$	$^{37}Ar/^{39}Ar$	$^{39}Ar_K$ (10^{-14}, mol)	^{39}Ar (% of total)	Apparent age (Ma)
400	22·9034	0·0276	0·0595	99·19	1·07	302·9 ± 5·90
500	18·6586	0·0073	0·0745	236·08	3·61	336·0 ± 4·70
600	19·9941	0·0063	0·0316	305·57	6·90	366·1 ± 3·7
700	20·4162	0·0032	0·0185	839·40	15·96	390·1 ± 3·9
800	20·8262	0·0028	0·0132	860·45	25·22	399·5 ± 4·0
900	20·8751	0·0020	0·0102	1659·08	43·09	404·9 ± 4·2
980	20·7693	0·0026	0·0081	835·61	52·09	399·9 ± 4·0
1080	20·8971	0·0028	0·0146	679·56	59·42	400·8 ± 4·4
1180	21·2045	0·0038	0·0242	1057·32	70·81	401·0 ± 3·9
1280	20·8729	0·0025	0·0058	1492·20	86·88	402·3 ± 4·1
1400	20·8007	0·0022	0·0411	1217·60	100·00	402·7 ± 4·6

high-pressure blueschists and eclogites, in a suture zone that marks the closure of the ancient Qilian Ocean as a result of continental collision. Yang *et al.* (2002*b*) reported magmatic zircon SHRIMP ages of 533–568 (554 ± 17) Ma for a gabbro of an ophiolite suite, suggesting that the Qilian Ocean had been in existence for some time, perhaps back to the Late Proterozoic.

Several high-quality Ar–Ar plateau ages have been reported in the literature: 462 ± 1·3 Ma for phengite from a Grt–Omp–Gln–Phn schist; 455 ± 10 Ma and 448 ± 11 Ma for phengite from blueschists (Liou *et al.*, 1989; Wu *et al.*, 1993; Zhang *et al.*, 1997). These ages are interpreted to signify the end of the high-pressure metamorphism of the ONQ during the Late Ordovician. Considering the well-developed, and partially well-preserved, Silurian flysch formations and Early Devonian molasse in the North Qilian Mountains (Bureau of Geology and Mineral Resources of Qinghai Province, 1991; Song, 1996), it is reasonable to infer that the Qilian Ocean, which might have opened in the Late Proterozoic, closed at the end of the Ordovician (~440 Ma) as a result of continental collision, followed by a major phase of mountain-building, which continued until at least the Early Devonian.

Tectonic evolution of the North Qaidam UHP Belt (CNQ)

Coesite inclusions in zircon grains from the pelitic gneiss demonstrate that continental materials must have been subducted (or dragged) down to mantle depths in excess of 100 km. Moreover, abundant exsolution lamellae of rutile, two pyroxenes and sodic amphiboles in garnet, and of ilmenite in olivine suggest that the garnet peridotite in this UHP belt was exhumed from depths >200 km (Song *et al.*, 2004, 2005*a*). The rock assemblage in the CNQ UHP belt is typical of continental-type collision belts, and is comparable with UHP terranes elsewhere, including the Dabie–Sulu in central–east China (e.g. Liou *et al.*, 1996), the Western Gneiss Region of Norway (e.g. Carswell *et al.*, 2003), and the Kokchetav of Kazakhstan (e.g. Katayama *et al.*, 2001).

Geochemical data for eclogites in the CNQ UHP belt suggest that their protoliths are of OIB and MORB affinity and may represent subducted oceanic crust. For the CNQ eclogites, the SHRIMP zircon U–Pb age of 457 ± 7 Ma is within error of the age for the eclogite from the ONQ HP belt (464 ± 5·5 Ma). Coesite-bearing zircon grains from the CNQ pelitic gneiss yield a mean age of 423 ± 6 Ma, which is consistent with the SHRIMP ages of diamond-bearing UHP metamorphic zircon grains from garnet lherzolite and garnet-bearing dunite in the same belt (Song *et al.*, 2005*b*; see above). Although this age is some 40 Myr younger than the ages of metamorphic zircon in the enclosed eclogites, the lithological package unequivocally recorded the UHP metamorphism. The exhumed garnet peridotites clearly experienced mantle depths in excess of 200 km, whereas the exhumed granitic/pelitic gneisses (supracrustal rocks) and eclogites would seem to have reached mantle depths no less than ~100 km. The differences in both metamorphic ages and pressure conditions may provide clues concerning the history of oceanic lithosphere subduction, continental collision–subduction, and ultimate exhumation in the northern margin of the Tibetan Plateau in the Paleozoic.

Relationship between the ONQ and CNQ belts and tectonic implications

The similar MORB- and OIB-like protoliths for both the ONQ HP and CNQ UHP eclogites suggest that they could have been derived from the same oceanic lithosphere. SHRIMP dating of eclogitic zircon from both belts suggests that the host eclogites formed during essentially the same period (~480–450 Ma) of oceanic lithosphere subduction (to depths >60 km). The similar protoliths (oceanic crustal materials) and essentially the same formation ages suggest a probable genetic link between the two belts.

Geochronological studies on Precambrian basement rocks (Wan *et al.*, 2001) suggest that the North Qilian Suture Zone (ONQ) is the major boundary that separates the Alax Block, the western part of the North China Craton with predominantly Archaean basement to the north, from the Qilian Block of Proterozoic basement

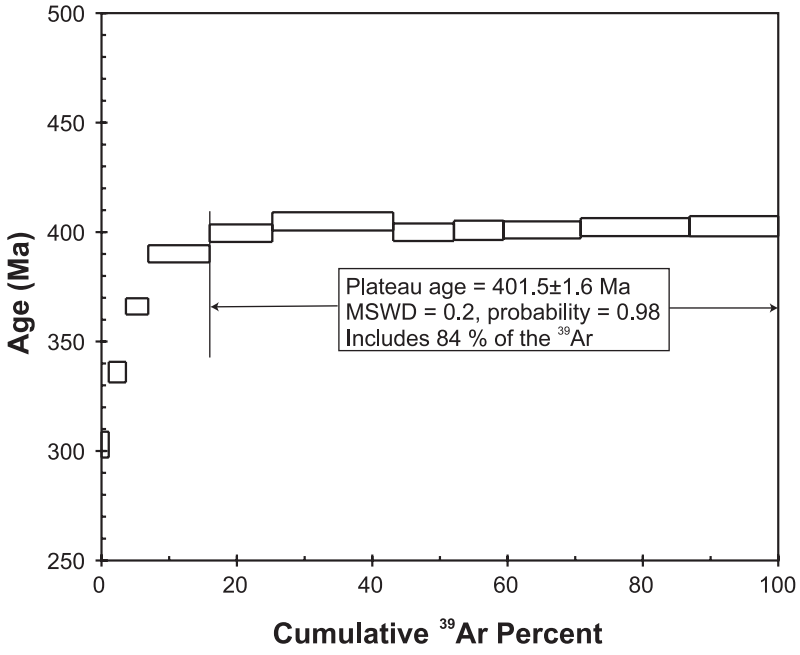

Fig. 10. Ar plateau age for white mica of the granitic gneiss 9Y117 from the CNQ UHP belt. Data are from Table 5.

rocks to the south. Zircon ages of granitic gneiss (992 ± 40 Ma, Song, 2001) and detrital zircon ages from a paragneiss (909–2192 Ma, 2C126) suggest that the protoliths of the UHP metamorphic gneisses formed part of the Qilian–Qaidam Craton, which subducted beneath the North China Craton, dragged by the downgoing oceanic lithosphere. The similarity of the Precambrian basement on both sides of the CNQ UHP metamorphic belt, together with its Devonian sedimentary cover (terrigenous sandstones and shales interlayered with marine limestones; Bureau of Geology and Mineral Resources of Qinghai Province, 1991), suggests that both the Qilian Block and the Qaidam Block may belong to the same stable Proterozoic 'craton' (informally referred to as the 'Qilian–Qaidam Craton'). The Qilian–Qaidam Craton may have had a passive continental margin with an extensive segment of attached oceanic lithosphere that subducted beneath the Alax Block of the North China Craton. Paleontological studies suggest that the North China Craton differs considerably from the Qilian–Qaidam Craton. This suggests the long-term existence of the Qilian Ocean prior to the Ordovician (Cui & Mei, 1997), although the size and detailed history of this ocean is unknown. Based on the characteristics of the Precambrian basement and zircon ages mentioned above, we infer that the Qilian–Qaidam Craton may be a fragment of the disintegrated Rodinia supercontinent (e.g. Li *et al.*, 2002), and that the North Qaidam UHP Belt does not necessarily represent the convergence zone of two major continents.

Figure 11 illustrates the inferred tectonic evolution of the ONQ and CNQ from oceanic lithosphere subduction, to continental collision and subsequent continental lithosphere underthrusting and ultimately exhumation. The Qilian Ocean may have existed in the Late Proterozoic, separating the North China Craton to the north and the Qilian–Qaidam Craton to the south. The Qilian–Qaidam Craton may be a fragment of the disintegrated Rodinia supercontinent with passive margins extending into oceanic lithosphere that floored the Qilian Ocean. The Qilian ocean floor may have subducted beneath the North China Craton forming a subduction-zone complex now represented by the ONQ. The northward drift of the Qilian–Qaidam Craton and continued subduction led to the collision of the two continents. The subducted and subducting oceanic lithosphere may have pulled the continental lithosphere, causing it to subduct or underthrust (similar to the present-day Indian plate underthrusting beneath Tibet) until the effect of the negative buoyancy diminished. Some eclogites of oceanic lithospheric fragments could have been entrained by the subducting continental crust. The presence of a positively buoyant sedimentary sequence (former accretionary trench sediments) might have led to the exhumation of the ONQ to the north, whereas positively buoyant continental crustal material could have resulted in the exhumation of the CNQ. This scenario satisfactorily explains the geological and geochemical observations as well as the ages of the various lithologies.

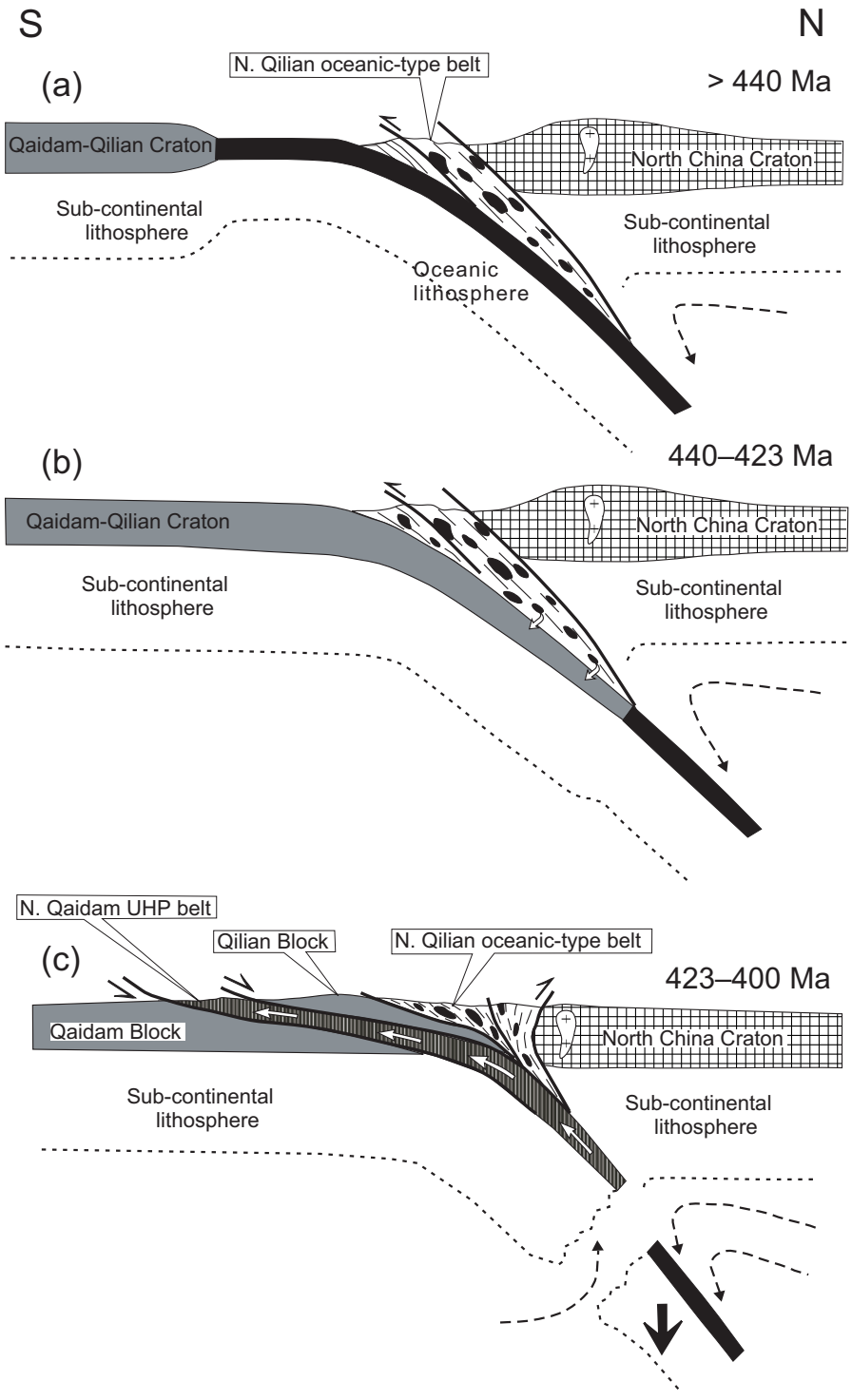

Fig. 11. A tectonic model that explains the genetic link between the ONQ HP and CNQ UHP belts and the Paleozoic tectonic evolution of the Northern Tibetan Plateau. (a) Subduction of North Qilian Ocean, which started in Early Ordovician (or earlier?) and closed along the North Qilian Suture Zone at about 460–440 Ma (Late Ordovician). (b) Qaidam–Qilian Craton started to subduct beneath the North China Craton dragged by the downgoing oceanic lithosphere and reached depths greater than 100 km at ~420 Ma. Some early eclogite blocks (oceanic fragments) were entrained by the subducted continental crust. (c) The UHP metamorphosed continental materials started to exhume when the positive buoyancy exceeded the drag of the subducted oceanic lithosphere (i.e. oceanic slab break-off) at ~400 Ma.

ACKNOWLEDGEMENTS

We would like to dedicate this paper to Dr S.-s. Sun, a great geoscientist, who made critical comments on an earlier version of this paper before he passed away. P. Jian and Y. H. Zhang are thanked for help in laboratory work during the SHRIMP dating, and X. M. Liu for his help on major and trace element analysis. We also thank Bradley Hacker and two anonymous reviewers for their detailed and rather constructive official review comments, and Geoffrey Clarke and Marjorie Wilson for smoothing the prose, which led to a better presentation of the final product. This work is financially supported by Natural Science Foundation of China (grants 40372031, 40272031, 40228003 and 40325005), Major State Basic Research Development Projects (G1999075508) and Key Laboratory Foundation of Northwest University to S.G.S.

REFERENCES

Bernard-Griffiths, J. & Cornichet, J. (1985). Origin of eclogites from south Brittany, France: an Sm–Nd isotopic and REE study. *Chemical Geology* **52**, 185–201.

Black, L. P., Kamo, S. L., Allen, C. M., Aleinikoff, J. N., Davis, D. W., Korsch, R. J. & Foudoulis, C. (2003). TEMORA 1: a new zircon standard for Phanerozoic U–Pb geochronology. *Chemical Geology* **200**, 155–170.

Bureau of Geology and Mineral Resources of Ningxia Province (1990). *Regional Geology of Ningxia Province. Geological Memoirs of Ministry of Geology and Mineral Resources of People's Republic of China.* Beijing: Geological Publishing House (in Chinese).

Bureau of Geology and Mineral Resources of Qinghai Province (1991). *Regional Geology of Qinghai Province. Geological Memoirs of Ministry of Geology and Mineral Resources of People's Republic of China.* Beijing: Geological Publishing House (in Chinese).

Carswell, D. A., Brueckner, H. K., Cuthbert, S. J., Mehta, K. & O'Brien, P. J. (2003). The timing of stabilisation and the exhumation rate for ultra-high pressure rocks in the Western Gneiss Region of Norway. *Journal of Metamorphic Geology* **21**, 601–612.

Compston, W., Williams, I. S., Kirschvink, J. L., Zhang, Z. & Ma, G. (1992). Zircon U–Pb ages for the Early Cambrian time-scale. *Journal of the Geological Society, London* **149**, 171–184.

Cui, Z. L. & Mei, Z. C. (1997). Middle Cambrian conodont fauna, paleoecology and tectonics of Qilian mountain. *Acta Palaeontologica Sinica* **36**, 86–92 (in Chinese with English abstract).

Dong, S. B., Shen, Q. H., Sun, D. Z. & Lu, L. Z. (1986). *The Metamorphic Map of China.* Beijing: Geological Publishing House.

Ernst, W. G. (2001). Subduction, ultrahigh-pressure metamorphism, and regurgitation of buoyant crustal slices—implications for arcs and continental growth. *Physics of the Earth and Planetary Interiors* **127**, 253–275.

Feng, Y. M. & He, S. P. (1995). Research for geology and geochemistry of several ophiolites in the North Qilian Mountains, China. *Geological Review* **40**, 252–264 (in Chinese with English abstract).

Gao, J. & Klemd, R. (2003). Formation of HP–LT rocks and their tectonic implications in the western Tianshan Orogen, NW China: geochemical and age constraint. *Lithos* **66**, 1–22.

Glassiey, W. (1974). Geochemistry and tectonics of Gressent volcanic rocks, Olympia Peninsula, Washington. *Geological Society of America Bulletin* **85**, 785–794.

Hermann, J., Rubatto, D. & Korsakov, A. (2001). Multiple zircon growth during fast exhumation of diamondiferous, deeply subducted continental crust (Kokchetav Massif, Kazakhstan). *Contributions to Mineralogy and Petrology* **141**, 66–82.

Katayama, I., Maruyama, S., Parkinson, C. D., Terada, K. & Sano, Y. (2001). Ion micro-probe U–Pb zircon geochronology of peak and retrograde stages of ultrahigh-pressure metamorphic rocks from the Kokchetav massif, northern Kazakhstan. *Earth and Planetary Science Letters* **188**, 185–198.

Kretz, R. (1983). Symbols for rock-forming minerals. *American Mineralogist* **68**, 277–279.

Li, H. M., Lu, S. N., Zheng, J. K., Yu, H. F., Zhao, F. Q., Li, H. K. & Zuo, Y. C. (2001). Dating of 3·6 Ga zircons in granite–gneiss from the eastern Altyn Mountains and its geological significance. *Bulletin of Mineralogy, Petrology and Geochemistry* **20**, 259–262 (in Chinese with English abstract).

Li, Z.-X., Li, X.-H., Zhou, H. & Kinny, D. (2002). Grenville-aged continental collision in South China: new SHRIMP U–Pb zircon results and implications for Rodinia configuration. *Geology* **30**, 163–166.

Liou, J. G., Wang, X. M. & Colemen, R. G. (1989). Blueschists in major suture zones of China. *Tectonics* **8**, 609–619.

Liou, J. G., Zhang, R. Y., Wang, X., Eide, E. A., Ernst, W. G. & Maruyama, S. (1996). Metamorphism and tectonics of high-pressure and ultrahigh-pressure belts in the Dabie–Sulu region, China. In: Yin, A. & Harrison, T. M. (eds) *The Tectonic Evolution of Asia.* Cambridge: Cambridge University Press, pp. 300–344.

Ludwig, K. R. (1991). Isoplot: a plotting and regression program for radiogenic isotope data. *US Geological Survey Open-File Report*, 91–445, pp. 37.

Maruyama, S., Liou, J. G. & Terabayashi, M. (1996). Blueschists and eclogites of the world and their exhumation. *International Geology Review* **38**, 485–594.

Mei, H. L., Yu, H. F., Lu, S. N., Lin, Y. X. & Li, Q. (1998). Archean tonalite in the Dunhuang, Gansu Province: age from the U–Pb single zircon and Nd isotope. *Progress in Precambrian Research* **21**, 41–45 (in Chinese with English abstract).

Meschede, M. (1986). A method of discriminating between different types of mid-ocean ridge basalts and continental tholeiites with the Nb–Zr–Y diagram. *Chemical Geology* **56**, 207–218.

Niu, Y. (2004). Bulk-rock major and trace element compositions of abyssal peridotites: surprises and implications for mantle melting, melt extraction and post-melting processes beneath ocean ridges. *Journal of Petrology* **45**, 2423–2458.

Niu, Y. & Batiza, R. (1997). Trace element evidence from seamounts for recycled oceanic crust in the eastern equatorial Pacific mantle. *Earth and Planetary Science Letters* **148**, 471–484.

O'Brien, P. J. (2001). Subduction followed by collision: Alpine and Himalayan examples. *Physics of the Earth and Planetary Interiors* **127**, 277–291.

Pearce, J. A. & Cann, J. R. (1973). Tectonic setting of basic volcanic rocks determined using trace element analysis. *Earth and Planetary Science Letters* **19**, 290–300.

Ratschbacher, L., Hacker, B. R., Calvert, A., Webb, L. E., Grimmer, J. C., McWilliams, M. O., Ireland, T., Dong, S. W. & Hu, J. M. (2003). Tectonics of the Qinling (Central China): tectonostratigraphy, geochronology, and deformation history. *Tectonophysics* **366**, 1–53.

Ravna, E. J. K. & Terry, M. P. (2004). Geothermobarometry of UHP and HP eclogites and schists—an evaluation of equilibria among

garnet–clinopyroxene–kyanite–phengite–coesite/quartz. *Journal of Metamorphic Geology* **22**, 579–592.

Rubatto, D. & Gebauer, D. (2000). Use of cathodoluminescence for U–Pb zircon dating by ion microprobe: some examples from the Western Alps. In: Pagel, M., Barbin, V., Blanc, P. & Ohnenstetter, D. (eds) *Cathodoluminescence in Geosciences*. Berlin: Springer, pp. 373–400.

Rubatto, D., Gebauer, D. & Compagnoni, R. (1999). Dating of eclogite-facies zircons: the age of Alpine metamorphism in the Sesia–Lanzo Zone (Western Alps). *Earth and Planetary Science Letters* **167**, 141–158.

Rudnick, R. L., Gao, S., Ling, W. L., Liu, Y. S. & McDonough, W. F. (2004). Petrology and geochemistry of spinel peridotite xenoliths from Hannuoba and Qixia, North China craton. *Lithos* **77**, 609–637.

Shervais, J. W. (1982). Ti–V plots and the petrogenesis of modern and ophiolitic lavas. *Earth and Planetary Science Letters* **59**, 101–118.

Song, S. G. (1996). *Metamorphic Geology of Blueschists, Eclogites and Ophiolites in the North Qilian Mountains. 30th IGC Field Trip Guide T392*. Beijing: Geological Publishing House, pp. 1–40.

Song, S. G. (2001). Petrology, mineralogy and metamorphic evolution of the Dulan UHP terrane in the North Qaidam, NW China and its tectonic implications. Doctoral thesis, Chinese Academy of Geological Science, Beijing (in Chinese).

Song, S. G., Yang, J. S., Xu, Z. Q., Liou, J. G. & Shi, R. D. (2003*a*). Metamorphic evolution of the coesite-bearing ultrahigh-pressure terrane in the North Qaidam, northern Tibet, NW China. *Journal of Metamorphic Geology* **21**, 631–644.

Song, S. G., Yang, J. S., Liou, J. G., Wu, C. L., Shi, R. D. & Xu, Z. Q. (2003*b*). Petrology, geochemistry and isotopic ages of eclogites in the Dulan UHPM terrane, the North Qaidam, NW China. *Lithos* **70**, 195–211.

Song, S. G., Zhang, L. F. & Niu, Y. L. (2004). Ultra-deep origin of garnet peridotite from the North Qaidam ultrahigh-pressure belt, Northern Tibetan Plateau, NW China. *American Mineralogist* **89**, 1330–1336.

Song, S. G., Zhang, L. F., Chen, J., Liou, J. G. & Niu, Y. L. (2005*a*). Sodic amphibole exsolutions in garnet from garnet-peridotite, North Qaidam UHPM belt, NW China: implications for ultradeep-origin and hydroxyl defects in mantle garnets. *American Mineralogist* **90**, 814–820.

Song, S. G., Zhang, L. F., Niu, Y. L., Su, L., Jian, P. & Liu, D. Y. (2005*b*). Geochronology of diamond-bearing zircons from garnet-peridotite in the North Qaidam UHPM belt, North Tibetan Plateau: a record of complex histories associated with continental collision. *Earth and Planetary Science Letters* **234**, 99–118.

Stacey, J. S. & Kramers, J. D. (1975). Approximation of terrestrial lead isotope evolution by a two-stage model. *Earth and Planetary Science Letters* **26**, 207–221.

Sun, S. S. & McDonough, W. F. (1989). Chemical and isotopic systematics of oceanic basalt: implications for mantle composition and processes: In: Saunders, A. D. & Norry, M. J. (eds) *Magmatism in the Ocean Basins. Geological Society, London, Special Publications* **42**, 313–345.

Tera, F. & Wasserburg, G. (1972). U–Th–Pb systematics in three Apollo 14 basalts and the problem of initial Pb in lunar rocks. *Earth and Planetary Science Letters* **14**, 281–304.

Vavra, G., Gebauer, D., Schmid, R. & Compston, W. (1996). Multiple zircon growth and recrystallization during polyphase Late Carboniferous to Triassic metamorphism in granulites of the Ivrea Zone (Southern Alps): an ion microprobe (SHRIMP) study. *Contributions to Mineralogy and Petrology* **122**, 337–358.

Wan, Y. S., Xu, Z. Q., Yan, J. S. & Zhang, J. X. (2001). Ages and compositions of the Precambrian high-grade basement of the Qilian Terrane and its adjacent areas. *Acta Geologica Sinica* **75**, 375–384.

Wu, H. Q., Feng, Y. M. & Song, S. G. (1993). Metamorphism and deformation of blueschist belts and their tectonic implications, North Qilian Mountains, China. *Journal of Metamorphic Geology* **11**, 523–536.

Yang, J. S., Xu, Z. Q., Song, S. G., Zhang, J. X., Wu, C. L., Shi, R. D., Li, H. B., Brunel, M. & Tapponnier, P. (2002*a*). Subduction of continental crust in the early Paleozoic North Qaidam ultrahigh-pressure metamorphism belt, NW China: evidence from the discovery of coesite in the belt. *Acta Geologica Sinica* **76**, 63–68.

Yang, J. S., Xu, Z. Q., Zhang, J. X., Song, S. G., Wu, C. L., Shi, R. D., Li, H. B. & Brunel, M. (2002*b*). Early Palaeozoic North Qaidam UHP metamorphic belt on the north-eastern Tibetan plateau and a paired subduction model. *Terra Nova* **14**, 397–404.

Zhang, J. X., Xu, Z. Q., Chen, W. & Xu, H. F. (1997). A tentative discussion on the ages of the subduction–accretionary complex/volcanic arcs in the middle sector of North Qilian Mountain. *Acta Petrologica et Mineralogica* **16**, 112–119 (in Chinese with English abstract).

Zhang, J. X., Zhang, Z. M., Xu, Z. Q., Yang, J. S. & Cui, J. W. (2001). Petrology and geochronology of eclogites from the western segment of the Altyn Tagh, Northwestern China. *Lithos* **56**, 187–206.

Zhang, J. X., Meng, F. C., Wan, Y. S., Yang, J. S. & Tung, K. A. (2003). Early Paleozoic tectono-thermal event of the Jingshuikou Group on the south margin of Qaidam: zircon U–Pb SHRIMP age evidence. *Geological Bulletin of China* **22**, 397–404 (in Chinese with English abstract).